UNIVERSIDADE ESTADUAL DE CAMPINAS
Faculdade de Engenharia Elétrica e de Computação
Jerson Alexis Pinzon Amorocho

Optimal Management of Energy Consumption and Comfort for Smart Buildings Connected to a Microgrid

Gestão Ótima do Consumo de Energia e do Conforto em Edificações Inteligentes Ligadas a uma Microrrede

Campinas

2018

UNIVERSIDADE ESTADUAL DE CAMPINAS
Faculdade de Engenharia Elétrica e de Computação

Jerson Alexis Pinzon Amorocho

Optimal Management of Energy Consumption and Comfort for Smart Buildings Connected to a Microgrid

Gestão Ótima do Consumo de Energia e do Conforto em Edificações Inteligentes Ligadas a uma Microrrede

Dissertação apresentada à Faculdade de Engenharia Elétrica e de Computação da Universidade Estadual de Campinas como parte dos requisitos exigidos para a obtenção do título de Mestre em Engenharia Elétrica, na Área de Energia Elétrica.

Supervisor: Prof. Dr. Luiz Carlos Pereira da Silva

Este exemplar corresponde à versão final da tese defendida pelo aluno Jerson Alexis Pinzon Amorocho, e orientada pelo Prof. Dr. Luiz Carlos Pereira da Silva

____

Campinas

2018

Agência(s) de fomento e nº(s) de processo(s): FAPESP, 2015/18145-0

Ficha catalográfica
Universidade Estadual de Campinas
Biblioteca da Área de Engenharia e Arquitetura
Luciana Pietrosanto Milla - CRB 8/8129

P658o

Pinzon Amorocho, Jerson Alexis, 1990-
Optimal management of energy consumption and comfort for smart buildings connected to a microgrid / Jerson Alexis Pinzon Amorocho. – Campinas, SP : [s.n.], 2018.

Orientador: Luiz Carlos Pereira da Silva.
Dissertação (mestrado) – Universidade Estadual de Campinas, Faculdade de Engenharia Elétrica e de Computação.

1. Edificações. 2. Sistemas de gestão de energia. 3. Otimização. I. Silva, Luiz Carlos Pereira da, 1972-. II. Universidade Estadual de Campinas. Faculdade de Engenharia Elétrica e de Computação. III. Título.

Informações para Biblioteca Digital

Título em outro idioma: Gestão ótima do consumo de energia e do conforto em edificações inteligentes ligadas a uma microrrede
Palavras-chave em inglês:
Buildings
Power management systems
Optimization
Área de concentração: Energia Elétrica
Titulação: Mestre em Engenharia Elétrica
Banca examinadora:
Luiz Carlos Pereira da Silva [Orientador]
Daniel Dotta
José Luiz Pereira Brittes
Data de defesa: 26-02-2018
Programa de Pós-Graduação: Engenharia Elétrica

COMISSÃO JULGADORA - DISSERTAÇÃO DE MESTRADO

Candidato: Jerson Alexis Pinzon Amorocho

RA: 163700

Data da Defesa: 26 de Fevereiro de 2018

Título da Tese: "Optimal Management of Energy and Comfort for Smart Buildings Connected to a Microgrid”.

Título da Tese em Português: “Gestão Ótima do Consumo de Energia e do Conforto em Edificações Inteligentes Ligadas a uma Microrrede”

Prof. Dr. Luiz Carlos Pereira da Silva (Presidente, FEEC/UNICAMP)

Prof. Dr. José Luiz Pereira Brittes (FCA/UNICAMP)

Prof. Dr. Daniel Dotta (FEEC/UNICAMP)

A ata de defesa, com as respectivas assinaturas dos membros da Comissão Julgadora, encontra-se no processo de vida acadêmica do aluno.

"Nadie puede decirte en quién te convertirás.
Solo tú, con los caminos que elijas tomar,
con cada vez que prefieras el querer sobre el deber,
con los obstáculos que te propongas vencer, con los sueños que hagas realidad y
con cada sonrisa que logres regalar o recibir de los demás;
te otorgarás la oportunidad que en cada ocasión que mires hacia atrás,
puedas ver tranquilamente el ser que has decidido forjar,
y notar que has llegado a dónde estabas destinado a llegar".

A Dios y mi mamá por su esfuerzo incansable
para darme las herramientas y enseñanzas para caminar por la vida.
A toda mi familia por estar siempre presentes en cada paso.
A ti Bonita, por mostrarme el mundo, ser el apoyo y la inspiración durante este viaje.
A mis amigos: Pedro, Nelly, David, Jeferson, Diego, Felipe, Silvia y Marcos,
por que hoy día más que mis amigos, son parte de mi familia.
Ao Prof. Luiz, pelo apoio constante para atinguir esta meta.
Obrigado por dar para mim a oportunidade de viver esta experiência.

Acknowledgements

This master's dissertation was supported by the São Paulo Research Foundation (FAPESP), under the research grant 2015/18145-0.

To my advisor, Prof. Dr. Luiz Carlos Pereira da Silva for his guidance and great support at every moment. To all the professors at the DSE/FEEC, especially to Prof. Dr. Marcos Rider for his contributions to this work.

To my friends and all my colleagues, particularly Pedro Pablo for his advice and important contributions to this work.

"Where there's a will, there's a way"

(Albert Einstein)

ABSTRACT

Buildings consume about 32% of the total electrical energy and are responsible for approximately 30% of CO_2 emissions worldwide. These facts have promoted the development of building energy management systems (BEMS), which integrate distributed generation (DG), demand response (DR) schemes and management of indoor conditions, to reduce energy consumption guaranteeing comfort requirements of the occupants. Additionally, if the BEMS operation is coordinated in conjunction with the electrical grid, events such as insufficient renewable-based generation, energy price fluctuations, voltage limits violations, among others, can be mitigated. Thereby, this master's dissertation presents a strategy to coordinate, in a centralized fashion, the operation of multiple buildings in a microgrid.

Initially, a BEMS to coordinate the operation of a smart building is developed, based on a mixed integer non-linear programming (MINLP) model, considering the management of heating, ventilation and air conditioning (HVAC) units, lighting appliances, photovoltaic generation (PV) and energy storage system (ESS), in order to minimize the total cost of energy consumption. Comfortable indoor conditions for the occupants are ensured by a set of mathematical constraints. Then, the mathematical representation of the electrical grid is integrated into the proposed MINLP model to extend the strategy to allow a central operator to manage the power consumption and generation of multiple buildings in a microgrid, with the aim of minimizing the total cost of the energy imported from the main utility, while operational constraints of the electrical grid are guaranteed. Additionally, a strategy that simplifies the original non-linear proposed model is presented, based on a set of linearization techniques and equivalent representations, obtained through a pre-processing stage executed in EnergyPlus. This strategy allows approximating the proposed MINLP model into a mixed integer linear programming (MILP) formulation, that can be solved using commercial solvers. In the First scenario of study, the proposed approach was tested individually in three buildings with different characteristics, without considering the electrical grid. The Second scenario of study included the entire model, analyzing a 13-bus microgrid with non-manageable loads and smart buildings. Finally, a rolling horizon (RH) strategy is proposed to address the uncertainty of the data, as well as reduce the amount of forecasting data required. Thus, in the Third scenario of study, the proposed RH scheme was tested in the same 13-bus microgrid, comparing the results with the solution found through the deterministic approach of the Second scenario.

Keywords: Smart buildings; microgrid; energy and comfort management; optimization.

RESUMO

As edificações consomem cerca de 32% da energia elétrica total e são responsáveis por cerca de 30% das emissões de CO_2 em todo o mundo. Estes fatos tem promovido o desenvolvimento de sistemas de gerenciamento de energia em edificações (BEMS), que integram sistemas de geração distribuída (DG), resposta à demanda (DR) e o gerenciamento de condições internas, a fim de reduzir o consumo de energia garantindo requisitos de conforto para os ocupantes. Além disso, se a operação do BEMS é coordenada com a rede elétrica, eventos como geração renovável reduzida, flutuações de preços de energia, violações de limites de tensão, entre outros, podem ser mitigados. Assim, esta dissertação de mestrado apresenta uma estratégia para coordenar, de forma centralizada, a operação de múltiplas edificações em uma microgrid.

Inicialmente, é desenvolvido um BEMS para coordenar a operação de um edifício inteligente, com base em um modelo de programação não linear inteira mista (MINLP), considerando a gestão de unidades de aquecimento, ventilação e ar condicionado (HVAC), aparelhos de iluminação, geração fotovoltaica (PV) e sistema de armazenamento de energia (ESS), a fim de minimizar o custo total do consumo de energia. Condições confortáveis para os ocupantes são asseguradas por um conjunto de restrições matemáticas. Em seguida, a representação matemática da rede elétrica é integrada no modelo MINLP proposto para ampliar a estratégia para permitir que um operador central gerencie o consumo de energia e a geração de múltiplas edificações em uma microgrid, com o objetivo de minimizar o custo total da energia importada da rede principal, enquanto as restrições operacionais da rede elétrica são garantidas. Além disso, é apresentada uma estratégia que simplifica o modelo não linear proposto, com base em um conjunto de técnicas de linearização e representações equivalentes, obtidas através de um estágio de pré-processamento executado no EnergyPlus. Esta estratégia permite aproximar o modelo MINLP proposto por meio de uma formulação de programação linear inteira mista (MILP), que pode ser resolvida usando softwares comerciais. No primeiro cenário de estudo, a abordagem proposta foi testada individualmente em três edificações com características diferentes, sem considerar a rede elétrica.O segundo cenário de estudo incluiu toda a modelagem, analisando uma microgrid de 13 barras com cargas não gerenciáveis e edificações inteligentes. Finalmente, uma estratégia de horizonte rolante (RH) é proposta para levar em conta a incerteza dos dados, bem como reduzir a quantidade de dados de previsão necessários. Assim, no terceiro cenário de estudo, o esquema de RH proposto foi testado na microgrid de 13 barras, comparando os resultados com a solução encontrada através da abordagem determinística do segundo cenário.

Palavras-chaves: Edificações inteligentes; microrrede; gestão de energia e conforto; otimização.

List of Figures

List of Tables

Notation

Sets:

$\mathcal{T}$	Set of time steps
$\mathcal{N}$	Set of buses
$\mathcal{L}$	Set of branches
$\mathcal{Z}_i$	Set of zones of the building i
$\mathcal{T}_{i,z}^{\kappa}$	Set of occupied time steps of the zone z of building i

Indexes:

z	Zone $z \in \mathcal{Z}_i$
t	Time interval $t \in \mathcal{T}$
i	Bus $i \in \mathcal{B}$
ij	Branch $ij \in \mathcal{L}$
λ	λth block used for the piecewise linearization

Parameters:

α_t	Energy price, [\$/kWh]
$A_i^{\boldsymbol{PV}}$	Area of the PV array, [m^2]
$\underline{C}_i$	Minimum permissible comfort index
$c^{\boldsymbol{Air}}$	Specific heat of the air, [kJ/kg^{o}C]
$\rho^{\boldsymbol{Air}}$	Density of the air, [kg/m^3]
$\boldsymbol{COP}_{i,z}$	Coefficient of performance of each HVAC unit, [W/W]
Δt	Duration of the time step
$\overline{\delta}_{i,z}^{I}$, $\overline{\delta}_{i,z}^{T}$	Discretization steps of the piecewise linearization of $\Delta_{i,z,t}^{I}$, $\Delta_{i,z,t}^{T}$
$\overline{\delta}_{ij}^{P}$, $\overline{\delta}_{ij}^{Q}$	Discretization steps of the piecewise linearization of $P_{ij,t}$, $Q_{ij,t}$
$\delta^{T_{\boldsymbol{Fan}}}$	Fan rise in air temperature, [^{o}C]
$\delta_{i,z,t}^{\boldsymbol{Srf}}$	Heat increment used to define $q_{i,z,t}^{Srf}$, [W]
E_i^B	Nominal energy of the ESS, [kWh]
$\overline{E}_i^B$	Maximum charging/discharging energy of the ESS, [kWh]
η_i^B, $\eta_i^{\boldsymbol{PV}}$	Efficiency of the ESS and PV systems
$\eta_{i,z}^{\boldsymbol{Fan}}$	Efficiency of the fan motor
$\boldsymbol{fp}_i$	Building power factor
$\zeta_{i,z}$	Lighting especial allowance factor
G_t	Irradiance, [W/m^2]
γ_i^{op}	Maximum charge/discharge cycles of the ESS
$h^{\boldsymbol{Ed}}$	Heat gain of a single electrical device, [W]
$h^{\boldsymbol{Oc}}$	Heat gain of a single people, [W]
$I_t^{\boldsymbol{OUT}}$	Natural illuminance, [Lx]
$\kappa_{i,z,t}^{\boldsymbol{Oc}}$	Electrical devices usage profile
$\kappa_{i,z,t}^{\boldsymbol{Ed}}$	Occupancy profiles
β, $T_{\boldsymbol{STC}}$	Design parameters of the PV array
$I_{i,z,t}^{o}$	Illuminance set point in the preprocessing stage, [Lx]
$T_{i,z,t}^{o}$	Temperature set point in the preprocessing stage, [^{o}C]
$\boldsymbol{LP}_{i,z}$	Lighting power ratio, [W/Lx]
$\sigma_{i,z,y}^{\boldsymbol{I}}$	Slope of the λth block used for the piecewise linearization of $(\Delta_{i,z,t}^{I})^2$
$\sigma_{i,z,y}^{T}$	Slope of the λth block used for the piecewise linearization of $(\Delta_{i,z,t}^{T})^2$
$\sigma_{ij,y}^{P}$	Slope of the λth block used for the piecewise linearization of $P_{ij,t}^2$
$\sigma_{ij,y}^{Q}$	Slope of the λth block used for the piecewise linearization of $Q_{ij,t}^2$
ψ', ψ''	Parameters for the linear regression of $f_{i,z,t}^{SHR}$
$\mu o_{i,z}^{\boldsymbol{I}}$	Illuminance comfortable set point, [Lx]
$\underline{\mu o}_{i,z}^{\boldsymbol{I}}$	Minimum illuminance level, [Lx]
$\overline{\mu o}_{i,z}^{\boldsymbol{I}}$	Maximum illuminance level, [Lx]
$\mu o_{i,z}^{\boldsymbol{T}}$	Temperature comfortable set point, [^{o}C]
$\underline{\mu o}_{i,z}^{\boldsymbol{T}}$	Minimum temperature, [^{o}C]
$\overline{\mu o}_{i,z}^{\boldsymbol{T}}$	Maximum temperature, [^{o}C]
$P_{i,z}^{\boldsymbol{Fan}}$	Fan power, [W]

$P^{PV}_{i,t}$	Active power supplied by the PV, [kW]
$P^{b}_{i,t}$	Base load of building, [kW]
$\underline{P}^{HVAC}_{i,z}$	Minimum power of each HVAC unit, W
$\overline{P}^{HVAC}_{i,z}$	Maximum power of each HVAC unit, W
$q^{N}_{i,z}$	Rated total cooling capacity of each HVAC unit, [W]
$q^{Ed}_{i,z,t}$	Electrical devices heat gain, [W]
$q^{Oc}_{i,z,t}$	People heat gain, [W]
$q^{Srfo}_{i,z,t}$	Surfaces heat gain of the pre-processing stage, [W]
$q^{Loss}_{i,z,t}$	Thermal fan losses, [W]
R_{ij}, X_{ij}	Resistance and reactance of the branch ij, [Ω]
$F^{SHR}_{i,z}$	Nominal sensible heat ratio
$\underline{SOC}_{i}$	Minimum SOC of the ESS
$\overline{SOC}_{i}$	Maximum SOC of the ESS
$\upsilon_{i,z}$	Volume of the zone, [m^3]
$\tau\kappa^{Oc}_{i,z}$	Total period of occupancy per zone
T^{OUT}_{t}	Outside temperature, [^{o}C]
$\nu^{Inf}_{i,z}$	Infiltration flow rate, [m^3/s]
$\nu^{Fan}_{i,z}$	Ventilation flow rate, [m^3/s]
$\underline{V}, \overline{V}$	Minimum and maximum voltage limits, [V]
$V'_{i,t}$	Estimated value of the voltage magnitude
$\omega^{I}_{i}, \omega^{T}_{i}$	Weight factors of visual and thermal comfort
$\overline{\lambda}$	Number of blocks for the piecewise linearization
Z_{ij}	Impedance of the branch ij, [Ω]

Continuous Variables:

$C_{i,z}$	Global comfort index
$C^{P}_{i,z,t}$	Partial comfort index
$C^{I}_{i,z,t}$	Visual comfort factor
$C^{T}_{i,z,t}$	Thermal comfort factor
$\Delta^{I}_{i,z,t}$	Deviation from the illuminance comfortable set point
$\Delta^{T}_{i,z,t}$	Deviation from the temperature comfortable set point
$E^{CH}_{i,t}$	Charging energy of the ESS, [kWh]
$E^{DCH}_{i,t}$	Discharging energy of the ESS, [kWh]
$E^{I}_{i,z,t}$	Energy of lighting appliances, [Wh]
$E^{T}_{i,z,t}$	Energy of HVAC units, [Wh]
$F^{EIR}_{i,z,t}$	Energy input ratio of HVAC unit
$f^{CCT}_{i,z,t}$	Cooling capacity temperature modifier factor
$f^{CCF}_{i,z,t}$	Cooling capacity flow fraction modifier factor
$f^{EIT}_{i,z,t}$	Energy input ratio temperature modifier factor
$f^{EIF}_{i,z,t}$	Energy input ratio flow fraction modifier factor
$f^{SHR}_{i,z,t}$	Sensible heat ratio modifier factor
$I_{i,z,t}$	Zone illuminance set point, [Lx]
$I^{sqr}_{i,j,t}$	Squared of current through branch i, j, [A^2]
$F^{PLR}_{i,z,t}$	Part load ratio of HVAC unit
$P_{ij,t}$	Active power flow of branch ij, [kW]
$Q_{ij,t}$	Reactive power flow of branch ij, [kW]
$P^{BD}_{i,t}$	Active internal power balance of building i, [kW]
$Q^{BD}_{i,t}$	Reactive internal power balance of building i, [kW]
$P^{L}_{i,t}$	Active power demand of non-manageable load i, [kW]
$Q^{L}_{i,t}$	Reactive power demand of non-manageable load i, [kW]
$q^{Inf}_{i,z,t}$	Infiltration heat gain, [W]
$q^{Ven}_{i,z,t}$	Ventilation heat gain, [W]
$q^{L}_{i,z,t}$	Lighting appliances heat gain, [W]
$q^{Srf}_{i,z,t}$	Surfaces heat gain, [W]

$q^{\boldsymbol{Sto}}_{i,z,t}$ Heat stored in the air volume of the zone, [W]

$q^{\boldsymbol{S}}_{i,z,t}$ Sensible cooling load of each zone, [W]

$q^{\boldsymbol{T}}_{i,z,t}$ Total cooling capacity of the cooling coil, [W]

$F^{\boldsymbol{RTF}}_{i,z,t}$ Run time fraction of each HVAC unit

$\Gamma^{\boldsymbol{C}H}_{i,t}$ Variable used to represent $(b^{CH}_{i,t} \cdot b^{CH}_{i,t-1})$

$\Gamma^{\boldsymbol{D}H}_{i,t}$ Variable used to represent $(b^{DH}_{i,t} \cdot b^{DH}_{i,t-1})$

$SOC_{i,t}$ State of charge

$T_{i,z,t}$ Zone temperature set point, [^{o}C]

$V^{\boldsymbol{sqr}}_{i,t}$ Squared of voltage at bus i, [V^2]

Binary Variables:

$b^{\mathbf{CH}}_{i,t}$ Variable associated with the charging mode of the ESS

$b^{\mathbf{DH}}_{i,t}$ Variable associated with the discharging mode of the ESS

$u_{i,z,t}$ Control variable of the HVAC unit operation

Contents

1 Introduction

Buildings consume about 32% of total energy and are responsible for approximately 30% of CO_2 emissions worldwide [1]. Therefore, government, industrial and scientific communities are making important efforts to mitigate the increase in energy consumption of this sector and promote more efficient practices in the operation of buildings. Some countries have defined legal and economic incentives, adopting policies such as setting up all new buildings nearly to zero-energy consumption [2]. Also, research works as [3] have developed strategies to design incentive programs including loans, production tax credit, among others, to support buildings sustainability.

Particularly in Brazil, during the energy crisis at the beginning of the previous decade, the government was forced to implement a rationing planning. During this period, 86.8% of residential users adopted some kind of action to save energy without affecting their quality of life [4]. In the commercial sector, 56.3% of companies adopted strategies to meet the goals proposed by the government, reducing the consumption 19%, without affecting their productivity [5]. Among these strategies, energy management schemes were adopted by about 61% of companies, as shown in Fig. 1. This fact pointed out the key role of energy management strategies in improving the energy consumption of buildings in the country, thus, the interest in developing this kind of system increased. Particularly, multiple pilot projects have been carried out by companies of the energy sector such as Companhia Paranaense de Energia, which released the project Smart Energy Paraná in 2013, in order to build a smartgrid including smart meters, distributed generation (DG) and a "house of the future" equipped with a photovoltaic system (PV), an energy storage system (ESS), and home automation, among other technologies. Similarly, AES Eletropaulo released the project Digital Eletropaulo in 2014, aiming to build a smart home that considers energy management, micro-generation, demand response (DR), electric vehicles and smart metering [6]. In the academic field, until 2014, at least 80 Brazilian research institutions were involved with activities related to smartgrids. However, less than 15% were focused on energy management in buildings and user services.

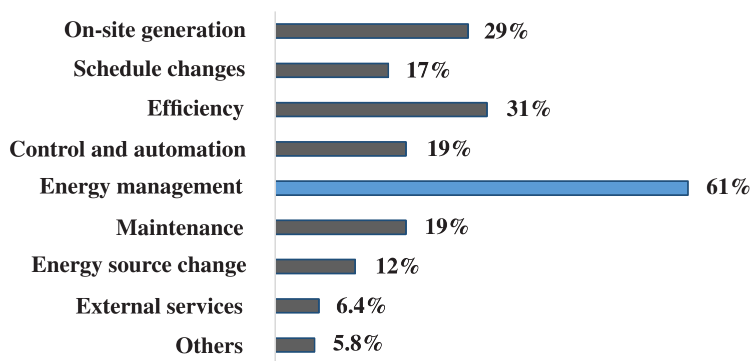

Figure 1 – Strategies adopted during the energy crisis in 2001, in Brazil [7].

In general, several strategies have been encouraged worldwide in order to make the operation of building more efficient. The usage of DG to supply the energy demand locally has increased. Several DR systems have been proposed, some of them based on the electricity price, market transactions or direct load control [8]. Additionally, ESSs such as batteries and thermal units have gained relevance to address the dynamics of renewable sources and the energy market [9]. In this context, building energy management systems (BEMS) have been developed to couple the energy consumption of buildings with DGs and ESS in short and long-term.

The implementation of BEMSs requires mathematical modeling and optimization techniques to coordinate the operation of multiple appliances to minimize the total cost of energy consumption. At this point, it is important to point out that energy saving is a goal that is in opposition to high comfort level for occupants [10], thus, BEMSs must manage the operation of buildings guaranteeing comfortable indoor conditions for the users. BEMSs must consider local weather conditions, particular features of the building such as windows and facade materials, characteristics of the activities performed by the occupants, clothes, among others. Finally, if the operation of multiple BEMSs is coordinated in conjunction with the electrical grid, events such as insufficient renewable-based generation, energy price fluctuations, voltage limits violations, among others, can be mitigated [11]. Practical cases of buildings interacting directly with the electrical distribution system to provide grid services can be found in [11, 12].

1.1 Objectives

The main objective of this master's dissertation is to develop a strategy to model and optimize, in a centralized fashion, the operation of multiple smart buildings (from now on, buildings) in a microgrid, considering the management of building loads (heat, ventilation and air conditioning (HVAC) units and lighting appliances), PV and ESS in conjunction with the features and technical constraints of the electrical grid, guaranteeing comfortable indoor conditions for the occupants. To do this, the following partial objectives are proposed:

- Developing a BEMS based on a detailed mixed integer non-linear programming (MINLP) model, describing the operation of HVAC units, lighting appliances, PV, ESS, thermal dynamics and a comfort index;
- Integrating a mathematical representation of the electrical grid into the proposed MINLP model to extend the energy management strategy in order to coordinate the operation of multiple buildings in a microgrid;
- Designing a strategy to approximate the original MINLP model and find an optimal solution for the operation of multiple buildings in a microgrid;

- Simulating the proposed strategy and studying technical aspects related to the operation of buildings, such as the relation between energy consumption and comfort, energy saving potential, energy management capacity, among others; as well as, technical aspects at the microgrid level such as voltage profile, peak power demand and power losses;
- Developing a rolling horizon (RH) strategy, which may be implemented in future real-time applications, in order to address the uncertainty of the data, as well as reducing the amount of forecasting data required.

1.2 Structure

This master's dissertation is structured as follows:

- Chapter 2 presents the concept of BEMS and a brief review of the strategies used in the literature to model the operation of buildings. Also, the proposed MINLP model to describe the operation of buildings is presented. In addition, a short review of trends regarding the interaction between buildings and the electrical distribution system is presented in conjunction with the mathematical representation of the electrical grid;
- Chapter 3 presents a strategy that simplifies the original MINLP model, based on a set of linearization techniques and equivalent representations, obtained through a pre-processing stage executed in the building energy evaluation tool EnergyPlus. This strategy allows approximating the proposed model into a mixed integer linear programming (MILP) formulation, that can be solved using commercial solvers;
- Chapter 4 presents the First scenario of study, which assumed the BEMS of each building operates individually. This scenario allows analyzing the operation of buildings as units, without considering the features of the electrical grid. Energy management capacity, energy saving potential, among other characteristics of buildings are studied. A Pareto Front is presented to describe the relationship between energy and comfort;
- Chapter 5 presents the Second scenario of study, which considered the operation of a 13-bus microgrid including non-manageable loads and buildings. This scenario may represent a cluster of buildings in a campus university or military facilities, in which all the participants share the same goal, to minimize the total cost of the energy imported from the main utility. Technical aspects of the electrical grid as voltage profile, peak power demand, and power losses are studied. Finally, a validation of the proposed strategy is presented, comparing the results obtained by the approximated MILP formulation and the solution of the non-linear power flow formulation in conjunction with simulations executed in EnergyPlus;

- Chapter 6 presents the Third scenario of study and the proposed RH strategy, which may be implemented to address the uncertainty and amount of forecasting data. The proposed RH scheme is based on a short horizon with discretized time steps and a long horizon with continuous time steps. The performance of this strategy is evaluated comparing its results with the solutions found in the Second scenario of study;

- Chapter 7 presents the main findings and conclusion of this dissertation in conjunction with some proposed topics and activities for future work.

2 Proposed MINLP Model

2.1 Building Energy Management System

A building energy management system is responsible for monitoring and controlling mechanical and electrical equipment to enhance the building efficiency by reducing the energy consumption [13]. For instance, in [14–16], multiple strategies are proposed to model and optimize the operation of HVAC systems. However, energy saving is an objective that is in opposition to high comfort level for occupants. The climate within a building is directly linked to the well-being and productivity of its users, thus, the decisions made by the BEMS must guarantee comfortable conditions for the occupants. In [10], it is presented an optimal Pareto Front describing the relation between energy consumption and comfort in buildings.

On the other hand, the increase of DG and ESS usage in buildings has added another task to BEMS: to coordinate building energy consumption with the energy available from DGs and ESS. This coordination has been studied by works as [17, 18]. In [17], it is presented a control strategy to couple an energy production system management, a DR system and the automation system of a large building equipped with micro-generation at the University of Évora, in Portugal. In [18], the ESS and HVAC system of a building are joined by a co-scheduling algorithm, reducing the electricity bill of the building by 15%.

The implementation of BEMSs requires mathematical representations to describe the operation of internal appliances, building thermal dynamics, comfort of the occupants, DG, ESS and other energy resources. In the literature, three modeling approaches have been used to represent the building operation: data-driven models [19], thermal resistance-capacitance (R-C) representations [20, 21], and high fidelity physical formulations [9, 22–24]. Data-driven models are based on large historical data, they provide good performance when operating with the trained data set. However, the inaccuracy of these models can increase when events outside the trained set occur. As for R-C models, they are used to represent a simplified form of physical phenomena, providing an accurate prediction of important building thermal states [20]. Nevertheless, the estimation of the parameters of these models requires complex characterization procedures [25].

High fidelity physical models capture accurate thermal interactions of buildings by using complex mathematical formulations. For instance, in [9], a detailed model to describe the thermal dynamics of a building is presented. The interaction between the building and different energy storage technologies is studied. In [22], a mixed integer linear programming (MILP) model is used to manage electrical and thermal resources aiming to minimize the total cost of the energy consumption of multiple houses, coordinating the operation of PV, ESS, a combined heat and power (CHP) unit and thermal storage. In [23], a co-simulation strategy is proposed to execute an iterative method to find the optimal operation of HVAC units, PV and ESS, simulating a candidate solution in EnergyPlus at each iteration. A similar approach is presented in [24]. The main disadvantages of these models are related to their size and complexity, requiring a large processing time. In general, these formulations cannot be easily incorporated into on-line optimization schemes, which are responsible for the energy management decisions in the operation of buildings [20].

Considering all the discussion presented above, this dissertation develops a detailed high fidelity physical MINLP model that can be incorporated into a BEMS to manage HVAC units, lighting appliances, PV and ESS of buildings, while comfortable indoor conditions for the occupants are kept by a set of mathematical constraints.

2.2 Proposed MINLP model of buildings operation

This section describes the mathematical modeling of the building operation. The proposed model is used by the BEMS in order to model and optimize the operation of several appliances. It is assumed the BEMS of each building manages the infrastructure that makes possible to control each HVAC unit and lighting system in the zones, PV and ESS. Buildings can extract or inject energy to the grid. Moreover, it is assumed that the BEMS gathers all the information required to solve the building operation problem. This information is similar to the data required by a typical energy building analysis tool, comprising weather data, technical information of the HVAC and lighting appliances, occupancy profiles and forecasted energy price.

2.2.1 Internal Power Balance of Buildings

The internal power balance of each building is defined by (2.1), as function of the building loads and energy resources. Building power consumption is composed by the demand of HVAC units ($E^{T}_{i,z,t}/\Delta t$), lighting system ($E^{I}_{i,z,t}/\Delta t$), and non-manageable internal demand ($P^{BL}_{i,t}$), which represents appliances such as computers, lighting of non-controlled areas, and other ancillary service devices; a detailed model of the building energy consumption is presented in Sec.2.2.2. Also, each building is equipped with a PV array, which power generation is represented by the term $P^{PV}_{i,t}$, while $E^{DC}_{i,t}$ and $E^{DH}_{i,t}$ represent the charging/discharging energy of the building ESS composed by a batteries bank. On the other hand, the reactive power demand of each building is defined by (2.2), depending on the active power consumption and the power factor (fp_i), which is considered to be constant.

$$P_{i,t}^{BD} = \frac{\sum_{z \in \mathcal{Z}_i} \left(E_{i,z,t}^{T} + E_{i,z,t}^{I}\right)}{\Delta t} + P_{i,t}^{BL} - P_{i,t}^{PV} - \frac{\eta_i^{B}\left(E_{i,t}^{DH} + E_{i,t}^{CH}\right)}{\Delta t} \tag{2.1}$$

$$Q_{i,t}^{BD} = \left[P_{i,t}^{BL} + \frac{\sum_{z \in \mathcal{Z}_i} \left(E_{i,z,t}^{T} + E_{i,z,t}^{I}\right)}{\Delta t}\right] \sqrt{\frac{1}{fp_i^2} - 1} \tag{2.2}$$

PV generation is modeled as in (2.3), based on forecasted irradiance (G_t) and temperature (T_t^{OUT}). The ESS is modeled using (2.4)–(2.11), as in [26]. The state of charge is defined as in (2.4). Charging/discharging states are defined through the binary variables $b_{n,t}^{\mathrm{CH}}$, $b_{n,t}^{DH}$ in (2.5)–(2.6). Constraint in (2.7) is used to model the unimodality operation of the ESS, i. e., the requirement to operate in only one state (charging, discharging or stand-by). According to [18], the state-of-health of the ESS is associated with the number of charge/discharge cycles and the state of charge ($SOC_{i,t}$), therefore, constraints (2.8)–(2.10) establish the maximum number of charging/discharging cycles, the value of $SOC_{i,t}$ at the end of the total horizon and the SOC limits, respectively.

$$P_{i,t}^{PV} = \eta_i^{PV} A_i^{PV} G_t \left[1 - \beta\left(T_t^{OUT} - T^{STC}\right)\right] \tag{2.3}$$

$$SOC_{i,t} = SOC_{i,t-1} + \frac{E_{i,t}^{CH} - E_{i,t}^{DH}}{E_i^{N}} \tag{2.4}$$

$$E_{i,t}^{CH} \leq \overline{E}_i^{B} b_{i,t}^{CH} \tag{2.5}$$

$$E_{i,t}^{DH} \leq \overline{E}_i^{B} b_{i,t}^{DH} \tag{2.6}$$

$$b_{i,t}^{\mathrm{CH}} + b_{i,t}^{DH} \leq 1 \tag{2.7}$$

$$\sum_{t \in \mathcal{T}} (b_{i,t}^{CH} - (b_{i,t}^{CH} * b_{i,t-1}^{CH})) + (b_{i,t}^{DH} - (b_{i,t}^{DH} * b_{i,t-1}^{DH})) \leq \gamma_i \tag{2.8}$$

$$SOC_{i,\mathcal{T}} = SOC^{F} \tag{2.9}$$

$$\underline{SOC}_i \leq SOC_{i,t} \leq \overline{SOC}_i \tag{2.10}$$

$$b_{i,t}^{\mathrm{CH}}, b_{i,t}^{DH} \in \{0,1\} \tag{2.11}$$

2.2.2 Building Energy Consumption Model

Typically, HVAC system consumes about 40% of the total energy of buildings [24]. Similarly, lighting is considered one of the largest loads and often responsible for the major space heat gain in buildings [27], influencing the consumption of the HVAC system. Thus, the proposed model considers the management of these both appliances, in order to achieve energy saving.

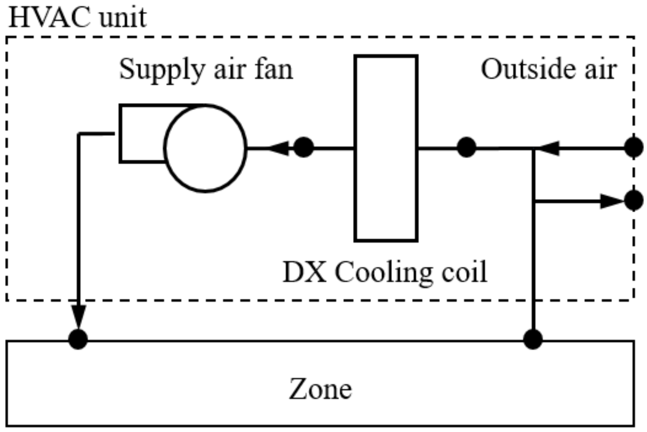

Figure 2 – Components of a single HVAC unit.

Each zone is equipped with an HVAC unit comprised by a single speed cooling coil and a constant volume fan as shown in Fig. 2. The HVAC unit consumption is described by (2.12), where the binary variable $u_{i,z,t}$ is used to model the state of the unit, i. e., $u_{i,z,t} = 1$ if the unit is active, otherwise $u_{i,z,t} = 0$. In (2.12), $F^{RTF}_{i,z,t}$ represents the fraction of the time step during which the unit works at full capacity, while the second term corresponds to the fan consumption. The total cooling capacity ($q^{T}_{i,z,t}$) and the energy input ratio ($F^{EIR}_{i,z,t}$) are adjusted by the modifier factors $f^{CCT}_{i,z,t}(q^{S}_{i,z,t})$, $f^{EIT}_{i,z,t}(q^{S}_{i,z,t})$, $f^{CCF}_{i,z,t}$, $f^{EIF}_{i,z,t}$ in (2.13) and (2.14), in order to consider the effect of weather conditions on the nominal cooling capacity ($q^{N}_{i,z}$) and the coefficient of performance ($COP_{i,z}$). These factors represent the HVAC performance curves used by the software tool EnergyPlus in [28], where $f^{CCF}_{i,z,t}$ and $f^{EIF}_{i,z,t}$ are represented by quadratic functions depending on the air volume fraction, while $f^{CCT}_{i,z,t}(q^{S}_{i,z,t})$ and $f^{EIT}_{i,z,t}(q^{S}_{i,z,t})$ are modeled as bi-quadratic functions depending on the wet-bulb temperature of the air entering the cooling coil and the dry-bulb temperature of the air entering the unit, more detailed information can be found in [28]. A strategy to approximate these factors is presented in the next Chapter (see Sec.3.1). Notice that, in the proposed model here, $f^{CCT}_{i,z,t}(q^{S}_{i,z,t})$ and $f^{EIRT}_{i,z,t}(q^{S}_{i,z,t})$ are described as function of $q^{S}_{i,z,t}$, i. e., the cooling load required by each zone (see Sec.2.2.3). Constraint (2.15) establishes the operational limits of each HVAC unit.

$$E^{T}_{i,z,t} = q^{T}_{i,z,t} F^{EIR}_{i,z,t} F^{RTF}_{i,z,t} \Delta t + u_{i,z,t} \cdot P^{Fan}_{i,z} \Delta t \tag{2.12}$$

$$q^{T}_{i,z,t} = f^{CCT}_{i,z,t}(q^{S}_{i,z,t}) \cdot f^{CCF}_{i,z,t} \cdot q^{N}_{i,z} \tag{2.13}$$

$$F^{EIR}_{i,z,t} = f^{EIRT}_{i,z,t}(q^{S}_{i,z,t}) \cdot f^{EIRF}_{i,z,t} / COP_{i,z} \tag{2.14}$$

$$u_{i,z,t} \cdot \underline{P}^{HVAC}_{i,z} \Delta t \leq E^{T}_{i,z,t} \leq u_{i,z,t} \cdot \overline{P}^{HVAC}_{i,z} \Delta t \tag{2.15}$$

$$u_{i,z,t} \in \{0, 1\} \tag{2.16}$$

Each zone is assumed to be equipped with dimmeable lighting appliances, which are controlled regulating the illuminance level set point ($I_{i,z,t}$), their energy consumption is expressed as a linear function in (2.17). The ratio $LP_{i,z}$ given in [W/Lx] can be obtained through simulations, measurements or technical catalogs.

$$E^{I}_{i,z,t} = LP_{i,z} I_{i,z,t} \Delta t \tag{2.17}$$

The energy consumption of internal non-manageable appliances is represented by the aggregated demand ($P^{BL}_{i,t}$). This demand profile can be obtained trough forecasting techniques or historical data.

2.2.3 Thermal Zone Model

The thermal balance of each zone is defined by (2.18), based on the model used by EnergyPlus in [28]; the heat gains considered in the balance are depicted in Fig. 3. The HVAC unit supplies the cooling load $q^{S}_{i,z,t}$ required by the zone, in order to maintain the temperature in the value defined by the set point ($T_{i,z,t}$). Sensible heat gains $q^{Oc}_{i,z,t}$, $q^{Ed}_{i,z,t}$, $q^{I}_{i,z,t}$ take into account the heat emanated by occupants, electrical devices and lighting appliances, respectively; while $q^{Srf}_{i,z,t}$ represents the heat gain through the zone surfaces. The electrical devices usage ($\kappa^{Ed}_{i,z,t}$) and occupancy ($\kappa^{Oc}_{i,z,t}$) profiles in (2.19) and (2.20), can be obtained by forecasting techniques or operational data of the building. Air volume thermal inertia and infiltration heat gain are expressed by (2.22) and (2.23), respectively.

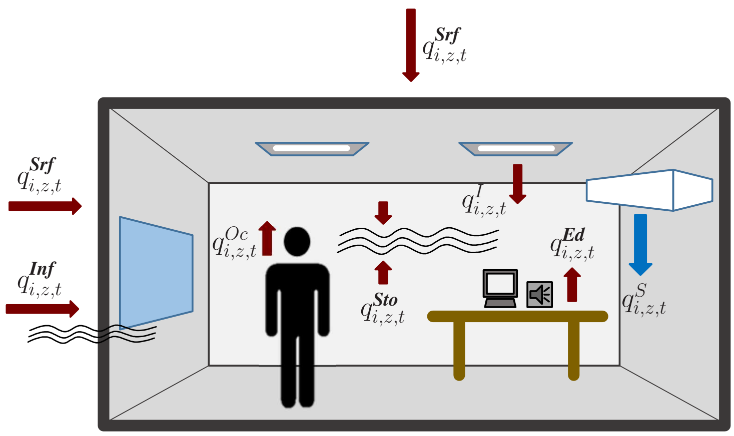

Figure 3 – Heat gains considered in the thermal balance of each zone.

$$q^{S}_{i,z,t} = \left(q^{Oc}_{i,z,t} + q^{Ed}_{i,z,t} + q^{I}_{i,z,t}\right) - q^{Sto}_{i,z,t} + q^{Inf}_{i,z,t} + q^{Srf}_{i,z,t} \tag{2.18}$$

$$q^{Oc}_{i,z,t} = h^{Oc} \kappa^{Oc}_{i,z,t} \tag{2.19}$$

$$q^{Ed}_{i,z,t} = h^{Ed} \kappa^{Ed}_{i,z,t} \tag{2.20}$$

$$q^{I}_{i,z,t} = \zeta_{i,z} E^{I}_{i,z,t} \tag{2.21}$$

$$q^{Sto}_{i,z,t} = \rho^{Air} c^{Air} \left(T_{i,z,t} - T_{i,z,t-1}\right) v_{i,z} \tag{2.22}$$

$$q^{Inf}_{i,z,t} = \rho^{Air} c^{Air} \left(T^{OUT}_{t} - T_{i,z,t}\right) \nu^{Inf}_{i,z} \tag{2.23}$$

2.2.4 Comfort Model

Lighting appliances and HVAC units are managed by the BEMS to achieve energy saving. However, they are directly linked to the thermal and visual indoor climate as well. Thus, the management of these appliances must also guarantee comfortable conditions for the occupants. To do this, the global comfort index ($C_{i,z}$) in (2.24) can be used, this formulation is based on the model proposed in [10]. This index calculates the average of the partial comfort index ($C^{P}_{i,z,t}$) during the total occupied period of each zone $\tau\kappa^{Oc}_{i,z}$. Based on this definition, $C_{i,z}$ equal 1 means that comfortable set points are strictly accomplished during all the occupied period. $C^{P}_{i,z,t}$ gathers the thermal ($C^{T}_{i,z,t}$) and visual ($C^{I}_{i,z,t}$) factors in (2.25). They quantify the deviation from predefined comfortable set points ($\mu o^{T}_{i,z}$ and $\mu o^{I}_{i,z}$), as modeled in (2.26) and (2.27). These deviations are based on the difference between the current set points ($T_{i,z,t}$ and $I_{i,z,t}$) and the comfortable predefined conditions, as defined in (2.28) and (2.29), they are considered only when the zone is occupied. The illuminance ($I^{OUT}_{i,z,t}$) is included to consider natural illumination, thus, the strategy can take into account both components, artificial and natural, to accomplish the desired illuminance level in the zone. Finally, (2.30) establishes the minimum permissible comfort $\underline{C}_i$, meanwhile constraints (2.31) and (2.32) keep $T_{i,z,t}$ and $I_{i,z,t}$ within comfortable ranges. It is important to highlight that this index represents a quantitative estimation of the comfort, however, other subjective aspects of the perception of the occupants can not be capture for this approach.

$$C_{i,z} = \frac{1}{\tau\kappa^{Oc}_{i,z}} \sum_{t \in \mathcal{T}^{\kappa}_{i,z}} C^{P}_{i,z,t} \tag{2.24}$$

$$C^{P}_{i,z,t} = \left(\omega^{T} C^{T}_{i,z,t}\right) + \left(\omega^{I} C^{I}_{i,z,t}\right) \tag{2.25}$$

$$C^{T}_{i,z,t} = 1 - \left(\frac{\Delta^{T}_{i,z,t}}{\mu o^{T}_{i,z}}\right)^{2} \tag{2.26}$$

$$C^{I}_{i,z,t} = 1 - \left(\frac{\Delta^{I}_{i,z,t}}{\mu o^{I}_{i,z}}\right)^{2} \tag{2.27}$$

$$\Delta^{T}_{i,z,t} = T_{i,z,t} - \mu o^{T}_{z} \tag{2.28}$$

$$\Delta^{I}_{i,z,t} = \left(I_{i,z,t} + I^{OUT}_{i,z,t}\right) - \mu o^{I}_{z} \tag{2.29}$$

$$C_{i,z} \geq \underline{C}_i \tag{2.30}$$

$$\underline{\mu o}_{i,z}^{T} \leq T_{i,z,t} \leq \overline{\mu o}_{i,z}^{T} \tag{2.31}$$

$$\underline{\mu o}_{i,z}^{I} \leq I_{i,z,t} + I_{i,z,t}^{OUT} \leq \overline{\mu o}_{i,z}^{I} \tag{2.32}$$

2.3 Buildings and Electrical Grid Interaction

Regarding the interaction between buildings and the electrical distribution system, few works have studied the effects of BEMS operation on the electrical grid and vice versa. Works such [20,29,30] have been focused on market approaches, particularly in [29], a combination of price and event based demand response is presented. This control scheme was tested modeling a small-sized apartment placed in Denmark. In [30], an information exchange framework to incorporate smart building demands into a microgrid operation is presented. In [20], two benchmark pricing methodologies are presented. Using dual decomposition, the authors propose distributing the cost of using the grid during the demand peak hours, abroad all the involved buildings. Nevertheless, in these works, little attention is given to the electrical grid modeling. In contrast, in [31], the impact of the operation of a building on the electrical distribution system is evaluated through indicators such as loss-of-load probability, a cover factor for supply and demand, among others. In [32], the mathematical modeling of the distribution grid is considered to study the operation of a microgrid with multiple buildings, although the proposed approach disregards PV and ESS operation, as well as the lighting system, which is considered one of the largest loads. Thereby, this dissertation includes a mathematical representation of the electrical grid in order to consider technical features and constraints of the electrical distribution system such as voltage limits, among others.

2.3.1 Electrical Grid Model

The proposed MINLP model aims to describe the operation of multiple buildings in a microgrid at the distribution level as the case presented in Fig. 4. It is considered the microgrid comprises buildings and non-manageable loads. The electrical grid is represented by the non-linear power flow equations defined in (2.33)–(2.38). Equations (2.33) and (2.34) model the active and reactive power balance, respectively. Here, $P_{i,t}^{L}$ and $Q_{i,t}^{L}$ represent the active and reactive non-manageable loads, meanwhile $P_{i,t}^{BD}$ and $Q_{i,t}^{BD}$ model the active and reactive internal power balance of the buildings[1], which were already presented in Sec. 2.2.1. The voltage drop in lines is represented by (2.35), while the definition of the current magnitude through lines is describe in (2.36). Finally, constraints (2.37) and (2.38) define the voltage and current magnitude limits, respectively.

[1] It is assumed that building i is connected to the bus $i \in \mathcal{N}$. Additionally, if there is no building or load at bus i, then $P_{i,t}^{BD} = Q_{i,t}^{BD} = 0$ and $P_{i,t}^{L} = Q_{i,t}^{L} = 0$.

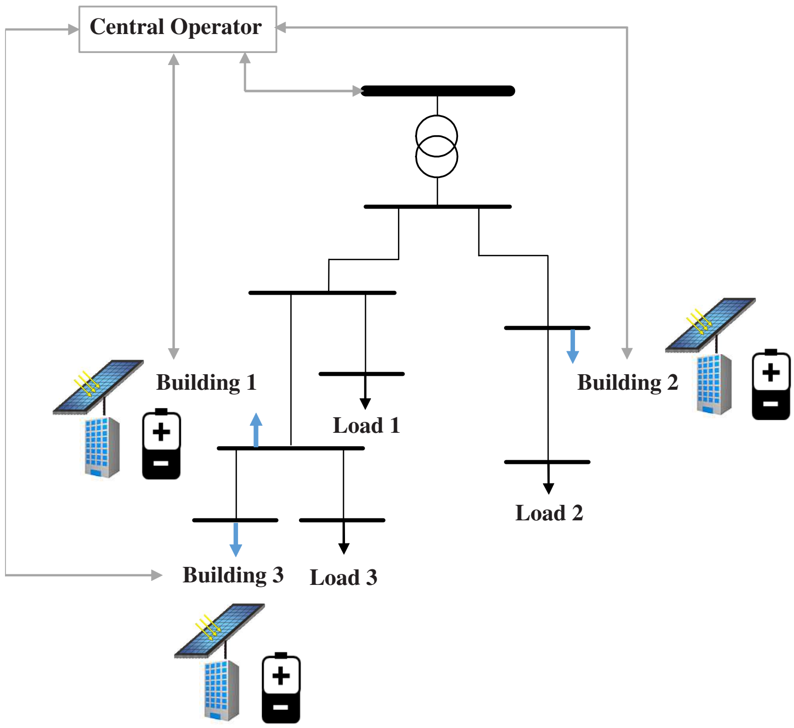

Figure 4 – Basic structure of a microgrid comprising multiple buildings and non-manageable loads.

$$\sum_{ji \in \mathcal{L}} P_{ji,t} - \sum_{ij \in \mathcal{L}} \left(P_{ij,t} + R_{ij} I_{ij,t}^2\right) = P_{i,t}^{BD} + P_{i,t}^{L} \tag{2.33}$$

$$\sum_{ji \in \mathcal{L}} Q_{ji,t} - \sum_{ij \in \mathcal{L}} \left(Q_{ij,t} + X_{ij} I_{ij,t}^2\right) = Q_{i,t}^{BD} + Q_{i,t}^{L} \tag{2.34}$$

$$V_{i,t}^2 - V_{j,t}^2 = 2\left(R_{ij} P_{ij,t} + X_{ij} Q_{ij,t}\right) - Z_{ij}^2 I_{ij,t}^2 \tag{2.35}$$

$$V_{i,t}^2 I_{ij,t}^2 = P_{ij,t}^2 + Q_{ij,t}^2 \tag{2.36}$$

$$\underline{V} \leq V_{i,t} \leq \overline{V} \tag{2.37}$$

$$I_{ij,t} \leq \overline{I}_{ij} \tag{2.38}$$

2.4 Objective Function

The mathematical model composed by (2.1)–(2.38) can be used by a central operator to coordinate the energy consumption and generation of the buildings in the microgrid, with the purpose of minimizing the total energy traded at the interconnection point microgrid-utility. This scenario may represent a cluster of buildings in a campus university or military facilities, in which all the participants share the same goal, which can be described as,

$$\min \quad \left\{ \sum_{t \in \mathcal{T}} \alpha_t \left[\sum_{i \in \mathcal{N}} P_{i,t}^{BD} \Delta t + \sum_{ij \in \mathcal{L}} R_{ij} I_{ij,t}^2 \Delta t \right] \right\} \tag{2.39}$$

The first term in (2.39) refers to the buildings internal energy balance (which can be negative if local generation is greater than consumption), while the second term refers to the active power losses in the electrical grid. Notice in (2.39) that aggregated loads ($P_{i,t}^L$) are not considered since they are non-manageable. The optimal operation (i. e., decision variables) is defined by the schedule of ESS charging/discharging profile ($E_{i,t}^{CH}$, $E_{i,t}^{DH}$), the temperature ($T_{i,z,t}$) and illuminance ($I_{i,z,t}$) set points in the zones of all the buildings, as well as the operational state of the HVAC units ($u_{i,z,t}$).

3 Proposed MILP Formulation and Solution Strategy

From a general point of view, the use of non-linear models and the several constraints involved, make the optimal operation of buildings a complex problem. The approaches that use simpler models allow obtaining analytic optimal solutions with a lower processing time but they can compromise the accuracy of the analysis [29]. On the other hand, the strategies based on non-linear models or building analysis tools can capture well the dynamics of the building but they have the disadvantage of performing high processing time and requiring a design phase to develop the building model. Particularly, finding an optimal solution to the MINLP model (2.1)–(2.39) is not easy due to the nature of the decision variables and complex methods used to estimate $f^{CCT}_{i,z,t}(q^S_{i,z,t})$, $f^{EIT}_{i,z,t}(q^S_{i,z,t})$ in (2.13) and (2.14), and $q^{Srf}_{i,z,t}$ in (2.18). Additionally, non-linear optimization techniques do not guarantee global optimality. Due this, it is proposed a strategy to approximate the original MINLP model into a MILP formulation, aiming to find an optimal solution to operate the buildings and microgrid. This strategy is composed by two stages: a pre-processing and an optimization stage, as explained next.

3.1 Pre-processing Stage

This stage is used to approximate $f^{CCT}_{i,z,t}(q^S_{i,z,t})$, $f^{EIT}_{i,z,t}(q^S_{i,z,t})$, and $q^{Srf}_{i,z,t}$, using a set of equivalent representations obtained through simulations executed in EnergyPlus [33]. This software was developed by the U.S. Department of energy, and it is widely used in research, design, planning analysis, and certification stages [34–36]. It can estimate the energy consumption of a building, calculates the heating and cooling loads required to control the temperature set points, taking into account the weather conditions and consumption of HVAC systems, lighting appliances and electrical devices. In real applications, the models developed in EnergyPlus are calibrated during initial stages using on-site real measurements, aiming to reduce the simulation errors. In this context, it is assumed that the building EnergyPlus models simulated as part of the scenarios of study in this dissertation are already calibrated.

At the beginning of the total horizon, each building is simulated using fixed set points $I^o_{i,z,t}$, $T^o_{i,z,t}$, and weather forecasting information. The results obtained are used to approximate $f^{CCT}_{i,z,t}(q^S_{i,z,t})$ and $f^{EIT}_{i,z,t}(q^S_{i,z,t})$ in (2.13) and (2.14). This approximation is suitable since constraints (2.31) and (2.32) keep the indoor conditions within predefined thresholds during the optimization process. In (2.12), $F^{RTF}_{i,z,t}$ can be approximated by the expression in (3.1), obtained through a linear regression, based on the model used by EnergyPlus in [28]. This approximation introduces a low error since the relation between $F^{RTF}_{i,z,t}$ and the part load ratio ($F^{PLR}_{i,z,t}$) is almost linear in the operational range of the HVAC unit, as shown in Fig.5. In (3.2), $F_{i,z,t}^{PLR}$ is defined as a function of the sensible cooling load required by the zone ($q_{i,z,t}^{S}$), the ventilation heat gain ($q_{i,z,t}^{Ven}$) and thermal losses ($q_{i,z,t}^{Loss}$). The sensible heat ratio modifier factor ($f_{i,z,t}^{SHR}$) is estimated using a linear regression based on the formulation presented in [37] and the results of the simulation using fixed set points. Finally, the ventilation heat gain is defined as in (3.3), while thermal losses due the air flow through the fan are presented in (3.4).

$$F_{i,z,t}^{RTF} = \psi' F_{i,z,t}^{PLR} + \psi'' \tag{3.1}$$

$$F_{i,z,t}^{PLR} = \frac{q_{i,z,t}^{S} + q_{i,z,t}^{Ven} + q_{i,z,t}^{Loss}}{f_{i,z,t}^{SHR} F_{i,z}^{SHR} q_{i,z,t}^{T}} \tag{3.2}$$

$$q_{i,z,t}^{Ven} = \rho^{Air} c^{Air} \left(T_t^{OUT} - T_{i,z,t} \right) \nu_{i,z}^{Fan} u_{i,z,t} \forall i, z, t \tag{3.3}$$

$$q_{i,z}^{Loss} = \left(1 - \eta^{Fan} \right) P_{i,z}^{Fan} u_{i,z,t} + \rho^{air} c^{Air} \delta^{T_{Fan}} \nu_{i,z}^{Fan} \tag{3.4}$$

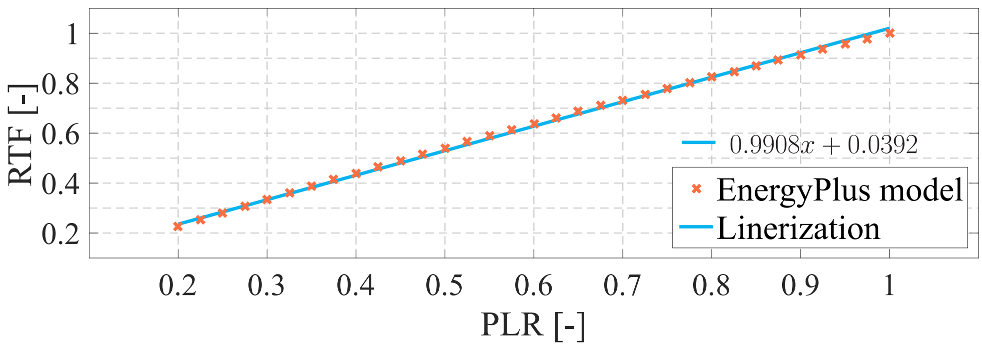

Figure 5 – Relation between the run time fraction $F_{i,z,t}^{RTF}$ and the part load ratio $F_{i,z,t}^{PLR}$.

The heat through the surfaces ($q_{i,z,t}^{Srf}$) in (2.18) is approximated by the linear function defined in (3.5). This expression is based on the heat through the surfaces obtained in the simulation ($q_{i,z,t}^{Srfo}$), which is adjusted according to the difference between the temperature set point used in the simulation ($T_{i,z,t}^{o}$) and the temperature set point ($T_{i,z,t}$), defined during the optimization process. $\delta_{i,z,t}^{Srf}$ represents the heat surfaces gain variation when $T_{i,z,t}$ changes 1^{o}C with respect to $T_{i,z,t}^{o}$. This parameter is calculated averaging the difference between $q_{i,z,t}^{Srfo}$ and the heat gain through the surfaces obtained from two additional simulations using the temperature set points ($T_{i,z,t}^{o} - 1^{o}C$) and ($T_{i,z,t}^{o} + 1^{o}C$). It is important to point out that this stage is executed in advance at the beginning of the time horizon, thus, the proposed simulations do not affect the processing time of the optimization process.

$$q_{i,z,t}^{Srf} = q_{i,z,t}^{Srfo} + \left(T_{i,z,t}^{o} - T_{i,z,t} \right) \delta_{i,z,t}^{Srf} \tag{3.5}$$

3.2 Optimization Stage

This stage aims to find an optimal solution to operate the buildings and microgrid guaranteeing the technical restrictions already mentioned. Before stating the final optimization model, it is necessary to define linear representations to approximate the remaining non-linear terms of the original MINLP model related to the ESS, the comfort index, the ventilation heat gain and the electrical grid.

3.2.1 ESS Linear Formulation

The product $b^{CH}_{i,t} \cdot b^{CH}_{i,t-1}$ in (2.8) can be replaced by the auxiliary variable $\Gamma^{CH}_{i,t}$, which is subject to (3.6)–(3.8). A similar approach can be carried out to linearize the product $b^{DH}_{i,t} \cdot b^{DH}_{i,t-1}$ as in (3.9)–(3.11).

$$\Gamma^{CH}_{i,t} \leq b^{CH}_{i,t} \tag{3.6}$$

$$\Gamma^{CH}_{i,t} \leq b^{CH}_{i,t-1} \tag{3.7}$$

$$b^{CH}_{i,t-1} + b^{CH}_{i,t-1} - 1 \leq \Gamma^{CH}_{i,t} \tag{3.8}$$

$$\Gamma^{DH}_{i,t} \leq b^{DH}_{i,t} \tag{3.9}$$

$$\Gamma^{DH}_{i,t} \leq b^{DH}_{i,t-1} \tag{3.10}$$

$$b^{DH}_{i,t-1} + b^{DH}_{i,t-1} - 1 \leq \Gamma^{DH}_{i,t} \tag{3.11}$$

3.2.2 Comfort Linear Formulation

The quadratic terms $(\Delta^{T}_{i,z,t})^2$ and $(\Delta^{I}_{i,z,t})^2$ in (2.26) and (2.27), can be linearized using the piecewise linear representation described in Fig.6. The parameter $\overline{\lambda}$ defines the amount of intervals used to approximate the variables. In this case, $(\Delta^{T}_{i,z,t})$ and $(\Delta^{I}_{i,z,t})$ are redefined as in (3.12) and (3.12), respectively. The required auxiliary variables are described in (3.14)–(3.22).

$$\Delta^{T}_{i,z,t} = \Delta^{T+}_{i,z,t} - \Delta^{T-}_{i,z,t} \tag{3.12}$$

$$\Delta^{I}_{i,z,t} = \Delta^{I+}_{i,z,t} - \Delta^{I-}_{i,z,t} \tag{3.13}$$

$$\Delta^{T+}_{i,z,t} + \Delta^{T-}_{i,z,t} = \sum\nolimits_{\lambda=1}^{\overline{\lambda}} \delta^{T}_{i,z,t,\lambda} \tag{3.14}$$

$$\Delta^{I+}_{i,z,t} + \Delta^{I-}_{i,z,t} = \sum\nolimits_{\lambda=1}^{\overline{\lambda}} \delta^{I}_{i,z,t,\lambda} \tag{3.15}$$

$$\delta^{T}_{n,z} = \left(\overline{\mu o}^{T}_{n,z} - \underline{\mu o}^{T}_{n,z}\right)/\overline{\lambda} \tag{3.16}$$

$$\delta^{I}_{n,z} = \left(\overline{\mu o}^{I}_{n,z} - \underline{\mu o}^{I}_{n,z}\right)/\overline{\lambda} \tag{3.17}$$

$$0 \leq \delta^{T}_{i,z,t,\lambda} \leq \overline{\delta}^{T}_{i,z} \tag{3.18}$$

$$0 \leq \delta^I_{i,z,t,\lambda} \leq \overline{\delta}^I_{i,z} \tag{3.19}$$

$$\Delta^{T+}_{i,z,t}, \Delta^{T-}_{i,z,t}, \Delta^{I+}_{i,z,t}, \Delta^{I-}_{i,z,t} \geq 0 \tag{3.20}$$

$$\sigma^T_{i,z,\lambda} = (2\lambda - 1)\overline{\delta}^T_{i,z} \tag{3.21}$$

$$\sigma^I_{i,z,\lambda} = (2\lambda - 1)\overline{\delta}^I_{i,z} \tag{3.22}$$

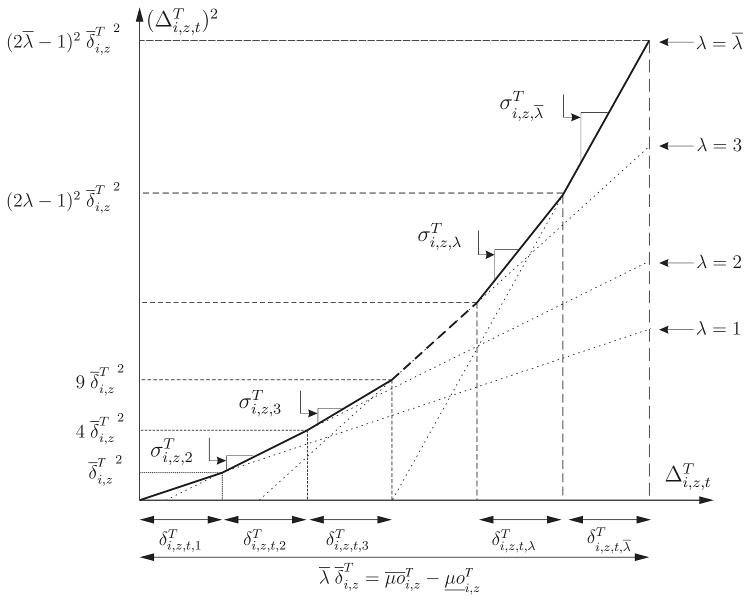

Figure 6 – Modeling the piecewise $\Delta^T_{i,z,t}$ linear function.

Thus, thermal and visual comfort factors in (2.26) and (2.27) can be rewritten as,

$$C^T_{i,z,t} = 1 - (\sum_{\lambda=1}^{\overline{\lambda}} \sigma^T_{i,z,\lambda}\delta^T_{i,z,t,\lambda})/(\mu o^T_{i,z})^2 \tag{3.23}$$

$$C^I_{i,z,t} = 1 - (\sum_{\lambda=1}^{\overline{\lambda}} \sigma^I_{i,z,\lambda}\delta^I_{i,z,t,\lambda})/\left(\mu o^I_{i,z}\right)^2 \tag{3.24}$$

3.2.3 Ventilation Heat Gain Linear Formulation

The product $T_{i,z,t} * u_{i,z,t}$ included in the representation of the ventilation heat gain in (3.3), can be replaced by the auxiliary variable $\Phi^T_{i,z,t}$ as in (3.25), using the disjunctive formulation defined in (3.26) and (3.27).

$$q^{Ven}_{i,z,t} = \rho^{Air} c^{Air} (T^{out}_t \nu^{Fan}_{i,z} u_{i,z,t} - \nu^{Fan}_{i,z} \Phi^T_{i,z,t}) \tag{3.25}$$

$$-\overline{\mu o}^T_{i,z} u_{i,z,t} \leq \Phi^T_{i,z,t} \leq \overline{\mu o}^T_{i,z} u_{i,z,t} \tag{3.26}$$

$$-\overline{\mu o}^T_{i,z}(1 - u_{i,z,t}) \leq \Phi^T_{i,z,t} - T_{i,z,t} \leq \overline{\mu o}^T_{i,z}(1 - u_{i,z,t}) \tag{3.27}$$

3.2.4 Electrical Grid Linear Formulation

The quadratic terms of the power flow formulation in (2.33)–(2.36) can be linearized by introducing the variables $V_{i,t}^{sqr}$ and $I_{ij,t}^{sqr}$ to represent $V_{i,t}^2$ and $I_{ij,t}^2$, respectively. On the other hand, in (2.36), $V_{i,t}^{sqr}$ can be replaced by its estimation $V'_{i,t}$ in order to approximate the product of the variables $V_{i,t}^{sqr}$ and $I_{ij,t}^{sqr}$. Finally, $P_{ij,t}^2$ and $Q_{ij,t}^2$, can be approximated using the piecewise linear formulation described in (3.28)–(3.38).

$$P_{ij,t}^T = P_{ij,t}^+ - P_{ij,t}^- \tag{3.28}$$

$$Q_{ij,t}^T = Q_{ij,t}^+ - Q_{ij,t}^- \tag{3.29}$$

$$P_{ij,t}^+ + P_{ij,t}^- = \sum_{\lambda=1}^{\overline{\lambda}} \delta_{ij,t,\lambda}^P \tag{3.30}$$

$$Q_{ij,t}^+ + Q_{ij,t}^- = \sum_{\lambda=1}^{\overline{\lambda}} \delta_{ij,t,\lambda}^Q \tag{3.31}$$

$$\delta_{ij}^P = \overline{P}_{ij}/\overline{\lambda} \tag{3.32}$$

$$\delta_{ij}^Q = \overline{Q}_{ij}/\overline{\lambda} \tag{3.33}$$

$$0 \leq \delta_{ij,t,\lambda}^P \leq \overline{\delta}_{ij}^P \tag{3.34}$$

$$0 \leq \delta_{ij,t,\lambda}^Q \leq \overline{\delta}_{ij}^Q \tag{3.35}$$

$$P_{ij,t}^+, P_{ij,t}^-, Q_{ij,t}^+, Q_{ij,t}^- \geq 0 \tag{3.36}$$

$$\sigma_{ij,\lambda}^P = (2\lambda - 1)\overline{\delta}_{ij}^P \tag{3.37}$$

$$\sigma_{ij,\lambda}^Q = (2\lambda - 1)\overline{\delta}_{ij}^Q \tag{3.38}$$

Then, (2.36) can be rewritten as the linear expression,

$$(V'_{i,t})^2 I_{ij,t}^{sqr} = (\sum_{\lambda=1}^{\overline{\lambda}} \sigma_{ij,\lambda}^P \delta_{ij,t,\lambda}^P) + (\sum_{\lambda=1}^{\overline{\lambda}} \sigma_{ij,\lambda}^Q \delta_{ij,t,\lambda}^Q) \tag{3.39}$$

3.3 Overview of the Solution Strategy and Proposed MILP formulation

The proposed strategy to find the optimal operation of multiple buildings in a microgrid is presented in Fig. 7. First, forecasting information about energy price, non-manageable loads of the microgrid, weather conditions, electrical devices usage and occupancy profiles, and non-manageable loads of buildings is gathered. Then, the pre-processing stage is executed for each building as explained in Sec.3.1. After that, the central operator executes the optimization stage using the results obtained in the pre-processing stage and the models presented in Sec.3.2. The linear model is implemented in AMPL [38] and solved with CPLEX [39]. The resulting linear problem to be solved by the central operator can be described as,

$$\min \quad (2.39),$$

Subject to: (2.1)–(2.2), (2.3), (2.4), (2.7)–(2.11), (2.17), (2.12)–(2.14), (2.18)–(2.23), (2.24)–(2.25), (2.28)–(2.32), (2.33)–(2.35), (2.37)–(2.38), (3.1)–(3.2), (3.4), (3.5), (3.6)–(3.11), (3.12)–(3.24), (3.25)–(3.27), (3.28)–(3.38), (3.39).

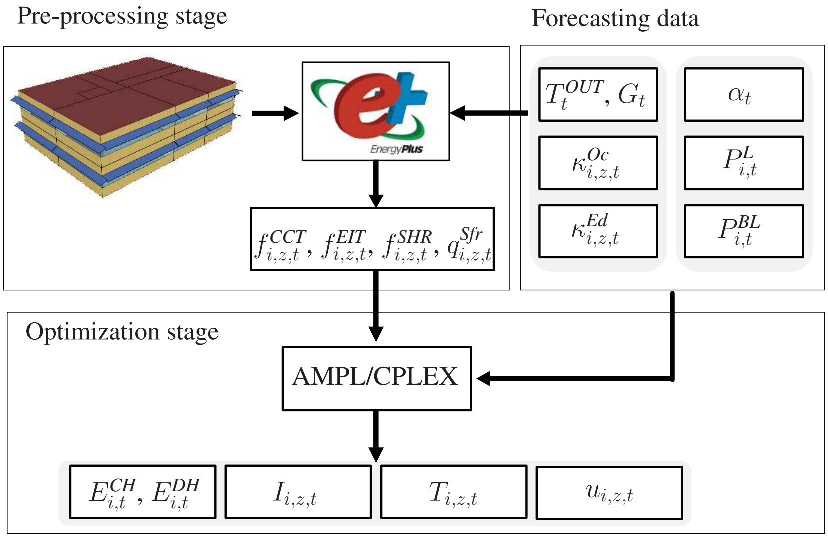

Figure 7 – Proposed solution strategy composed of a pre-processing and an optimization stage.

4 First Scenario of Study: Buildings Operating Individually

In order to assess the performance of the BEMS and the proposed model at building level, in the First scenario of study, it is considered that each building operates individually, aiming to optimize its own operation to reduce the total cost of energy consumption. To do this, the proposed strategy is executed without considering the electrical grid model or other buildings. Additionally, PV and ESS systems are not considered with the aim of analyzing the relation between the consumption management capacity and comfort directly. Thus, the objective function in 2.39 is modified to take into account only the term related to the consumption of each building as in 4.1. The problem to be solved for each building can be described as,

$$\min \quad \sum_{t \in \mathcal{T}} \alpha_t P_{i,t}^{BD} \Delta t \tag{4.1}$$

Subject to: (2.1)–(2.2), (2.3), (2.4), (2.7)–(2.11), (2.17), (2.12)–(2.14), (2.18)–(2.23), (2.24)–(2.25), (2.28)–(2.32), (2.33)–(2.35), (2.37)–(2.38), (3.1)–(3.2), (3.4), (3.5), (3.6)–(3.11), (3.12)–(3.24), (3.25)–(3.27).

The strategy was tested in three buildings considering a total horizon $\mathcal{T} = 24$h with 10min time steps. Each building has ten zones comprising classrooms, offices and computing rooms with different occupancy profiles. Table 1 summarizes general information related to the operation of each building (more detailed characteristics can be found in Appendix A). A database containing real weather information provided in [40] was used, while the forecasted energy price is shown in Fig. 8. The internal non-manageable demand is defined as 10% of the installed demand, during the operating time of each building, and 5% for the remaining hours as in Fig. 9. These values were defined taking into account that HVAC and lighting represent the largest loads in offices buildings, for other kinds of buildings the internal non-manageable demand may be bigger. This fact could limit the capability of the energy management system to optimize the building operation. The pre-processing stage was executed, with fixed temperature and illuminance set points, $T_{i,z,t}^{o} = 22.5^{o}C$ and $I_{i,z,t}^{o} = 500Lx$. The MILP model in the optimization stage was implemented in AMPL and solved with CPLEX, using a workstation with an Intel i7-4790 processor and 16 GB RAM.

Table 1 – First scenario of study. Buildings general information.

	Building 1	Building 2	Building 3
Usage	Classrooms	Technology	Offices
Operating time	[7:00-21:00h]	[8:00-18:00h]	[8:00-18:00h]
Zones	10	10	10

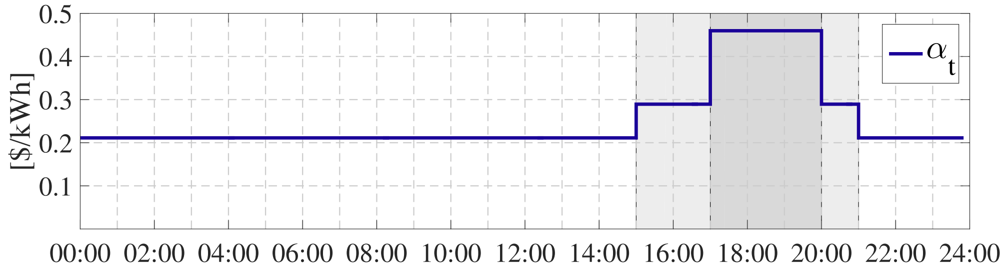

Figure 8 – Energy price. The high price period is 17:00-20:00h, while the middle price period comprises 15:00-17:00h and 20:00-21:00h. The remaining hours correspond to the low price period.

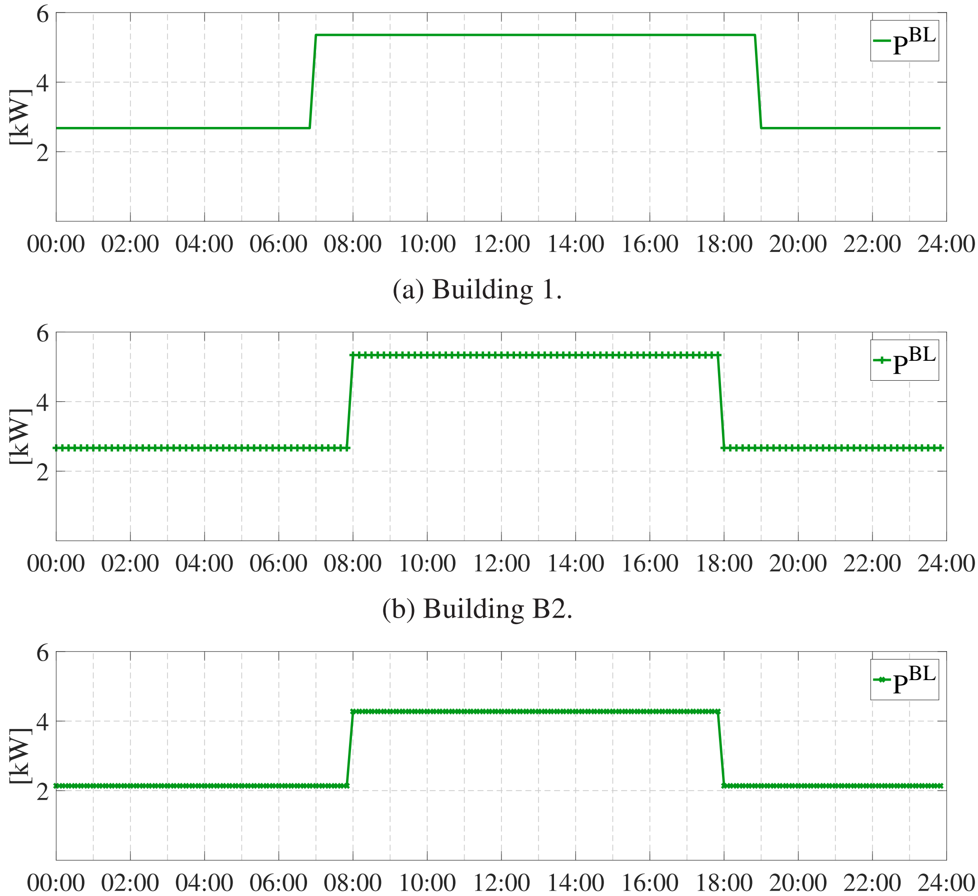

(a) Building 1.

(b) Building B2.

(c) Building B3.

Figure 9 – Non-manageable internal demand of the buildings analyzed.

Typically, the set points of HVAC and lighting appliances are fixed during the operating periods of the zones, this scheme limits the building consumption management capacity. With the purpose of studying the effect of relaxing those constraints, three cases considering only the management of HVAC and lighting appliances were studied. In Case I (base case) the indoor temperature and illuminance were defined as the typical set points presented in Table 2, meanwhile in cases II and III, the set points $T_{i,z,t}$ and $I_{z,t}$ were subject to take values into the comfortable ranges $[20-25]^o$C and $[400-600]$Lx, respectively. In Case II the minimum permissible comfort index $\underline{C}_i$ was defined as 0.995, allowing the BEMS to manage the HVAC and lighting appliances. In Case III the restriction over the comfort index is relaxed significantly defining $\underline{C}_i = 0.900$, in order to obtain a trivial solution, which makes all the zones of the building operate with the maximum temperature, and the lowest illuminance setpoint. In addition, the weight factors of thermal and visual comfort were defined as $\omega_i^I = \omega_i^T = 0.5$. All the cases of study can be described as,

Case I: Only consumption management, $T_{z,t}$ and $I_{z,t}$ fixed,
Case II: Only consumption management, $\underline{C} = 0.995$,
Case III: Only consumption management, $\underline{C} = 0.900$.

Table 2 – Comfortable indoor conditions.

	Typical set point	Comfortable range
Temperature*	$\mu o_{i,z}^T = 22.5^o$C	$[\underline{\mu o}_{i,z}^T, \overline{\mu o}_{i,z}^T] = [20-25]^o$C
Illuminance**	$\mu o_{i,z}^I = 500$Lx	$[\underline{\mu o}_{i,z}^I, \overline{\mu o}_{i,z}^I] = [400-600]$Lx

* Conditions for a summer day [41].
** Conditions for work areas in offices and similar spaces [42].

4.1 Buildings Consumption Management Capacity

Cases I, II and III do not include PV and ESS into the analysis in order to assess the buildings consumption management capacity. The comfort constraint plays an important role in the management decisions as can be seen in Fig. 10, which shows buildings power consumption. For all buildings, Case I describes the highest values due to its non-flexible operational scheme. In contrast, in Case II, HVAC and lighting appliances were managed to achieve energy saving. In this case, the total energy consumption of buildings was reduced 9.1%, 12.2% and 12.3%, respectively. Also, the peak power demand decreased, Table 3 summarizes the results obtained for each building.

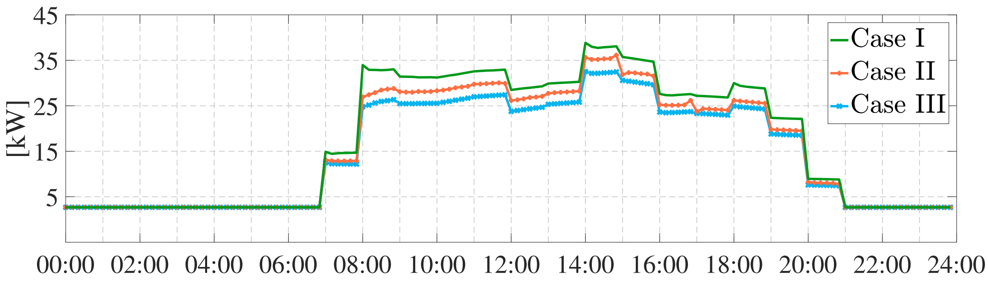

(a) Building 1.

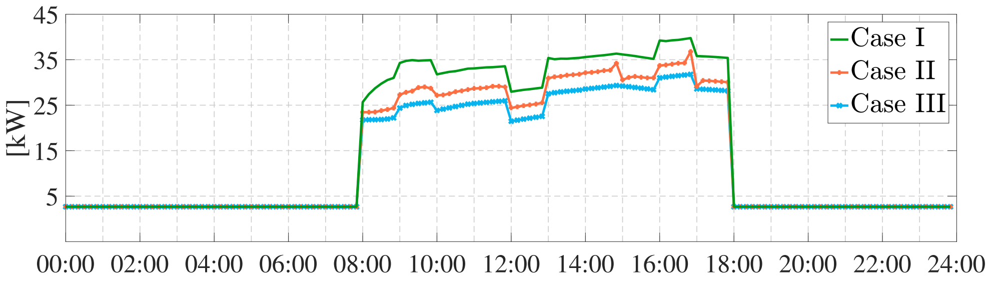

(b) Building B2.

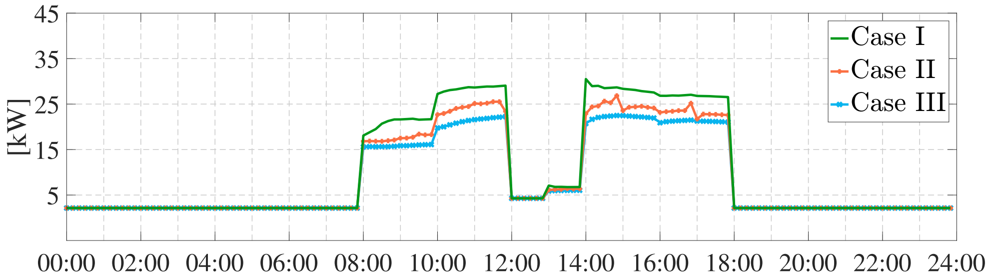

(c) Building B3.

Figure 10 – First scenario of study. Buildings power consumption. Cases I, II and III.

Table 3 – First scenario of study. Comparison results for cases I, II and III.

	Building 1			Building 2			Building 3		
Case	I	II	III	I	II	III	I	II	III
$\underline{C}$	1	0.995	0.900	1	0.995	0.900	1	0.995	0.900
Consumption [kWh]	417.5	379.6	353.3	377.0	330.8	302.2	250.2	219.3	200.9
Total Cost [$]	113.3	102.6	95.9	95.9	84.0	77.1	65.0	56.9	52.31
Peak power [kW]	38.8	36.1	32.4	39.7	36.8	31.8	30.5	26.8	22.4
HVAC [kWh]	236.5	201.8	189.2	190.5	147.5	134.8	113.5	84.8	77.0
Lighting [kWh]	84.5	81.4	67.6	95.8	92.6	76.7	64.0	61.8	51.2

Besides managing the HVAC units and lighting appliances to reduce the power consumption along the operating hours, the BEMS also reacts to the energy tariff policy. As mentioned before, high values of comfort index represent high power consumption; Fig. 11 shows the temperature and illuminance set points in zone 6 of building 1, for Case II. After 15:00h, temperature set point increases to reduce the consumption of the HVAC unit during the medium/high price period. Similarly, the illuminance set point decreases at 17:00h to reduce the consumption of the lighting appliances. Additionally, regarding the temperature dynamics in Fig. 11(a), it is possible to observe that temperature set point decreases at 14:50h and 16:50h, in order to take advantage of the mass volume inertia to storage cooling energy before the beginning of the medium and high price period. All the zones of the building operated in a similar fashion, executing a coordinated action to reduce the energy consumption during the medium/high price period.

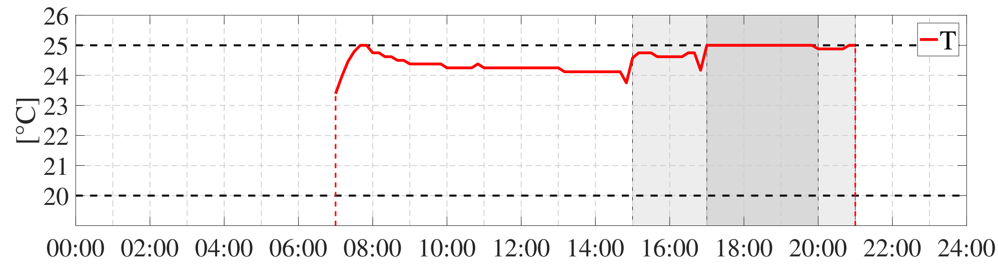

(a) Temperature set point.

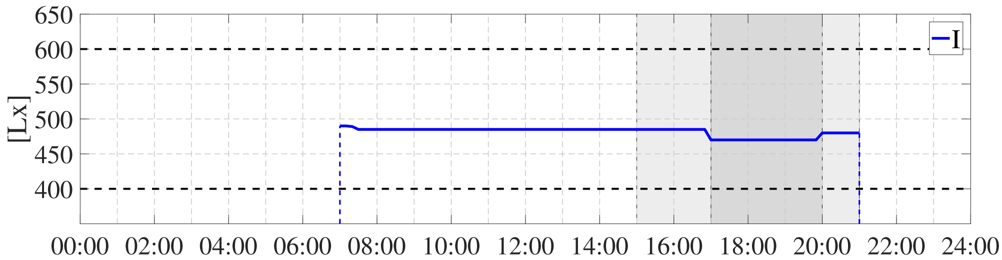

(b) Illuminance level set point.

Figure 11 – First scenario of study. Temperature and illuminance set points, zone 6 of Building 1 during the occupied periods. Case II.

This behavior can be described through the partial comfort index dynamics in Fig. 11 as well. During the low price period, $C_{i,z,t}$ was kept over 0.995 near to 1 in all the buildings. When the medium price period starts at 15:00h, $C_{i,z,t}$ decreased to minimize the HVAC and lighting appliances consumption. Later, at 17:00h when the high price period starts, the comfort index took lower values, aiming to reduce the purchased energy during this period. It is worth highlight that during all occupied periods, $T_{i,z,t}$ and $I_{i,z,t}$ were kept within the comfortable ranges $[20-25]^o$C and $[400-600]$Lx, while the global comfort index was limited by $\underline{C}_i = 0.995$. In total, the management decisions of the BEMS in Case II reduce the total cost of the operation of each building by 9.4%, 12.4% and 12.5%, respectively, when comparing with Case I.

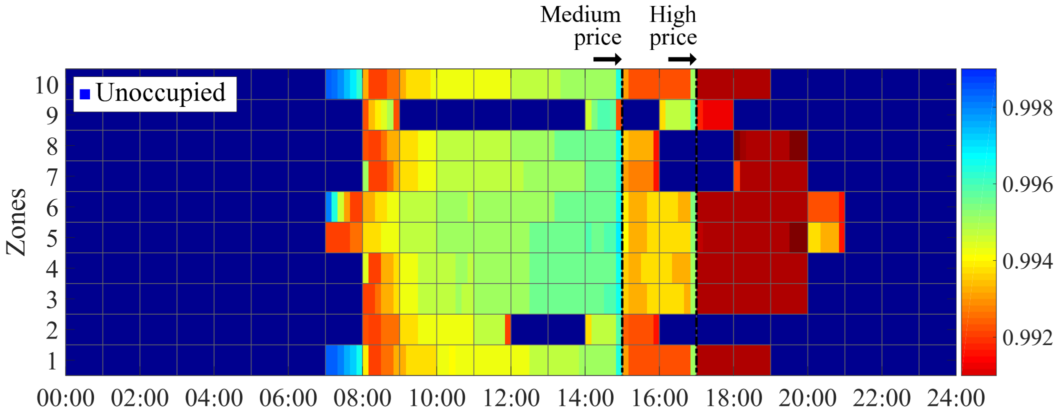

(a) Building 1.

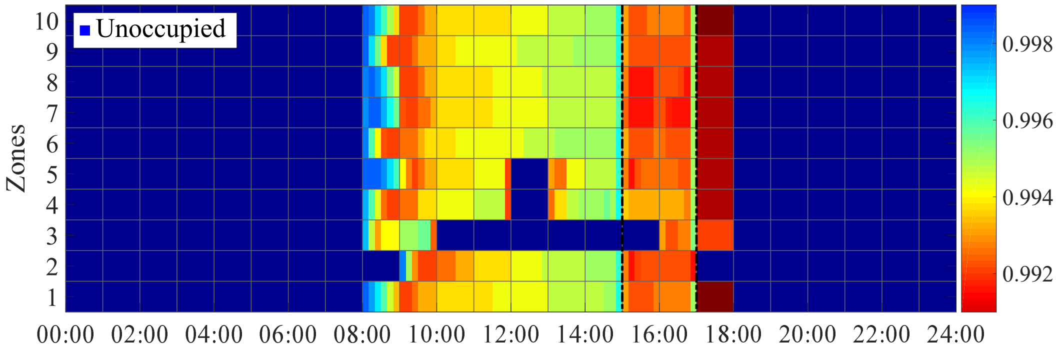

(b) Building B2.

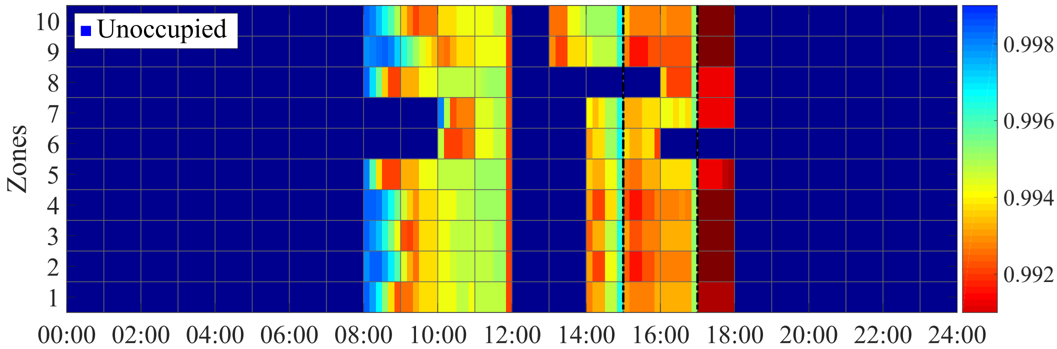

(c) Building B3.

Figure 12 – First scenario of study. Buildings comfort index dynamics. Case II.

In Case III, a trivial solution was obtained, all buildings operate with $T_{i,z,t} = 25^oC$ (upper limit) and $I_{i,z,t} = 400Lx$ (lower limit). In this case, the total consumption of the buildings was reduced 15.4%, 19.8% and 19.7%, respectively. While the total cost decreased 15.3%, 19.6% and 19.5%, respectively. As mentioned before, the comfort constraint is linked directly to the consumption management capacity. The relation between these factors can be seen in the Pareto Fronts presented in Fig. 13, here the total consumption of HVAC units and lighting appliances varies regarding the values of the minimum permissible comfort index. The more the comfort index value increases (limiting the consumption management capacity), the more the energy consumption increases. The maximum energy consumption occurs when the set points are fixed

($T_{i,z,t} = 22.5^oC$ and $I_{i,z,t} = 500Lx$), meanwhile the minimum energy consumption is obtained with the trivial solution ($T_{i,z,t} = 25^oC$ and $I_{i,z,t} = 400Lx$).

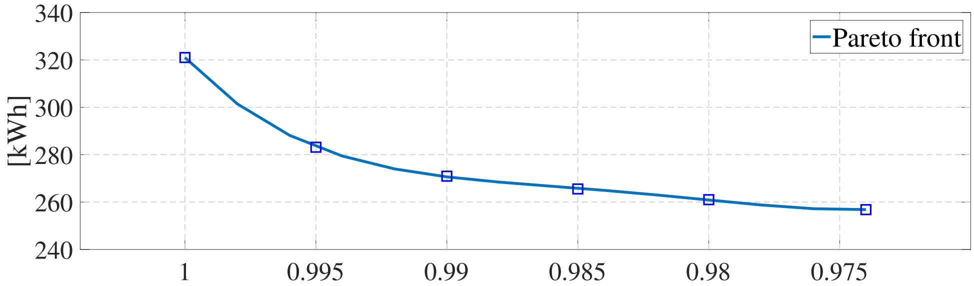

(a) Building 1.

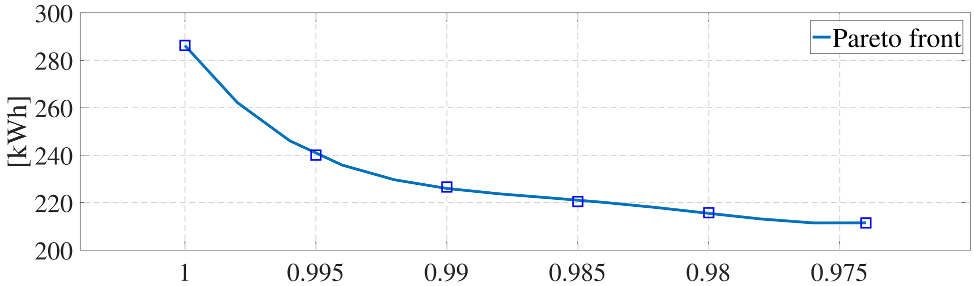

(b) Building B2.

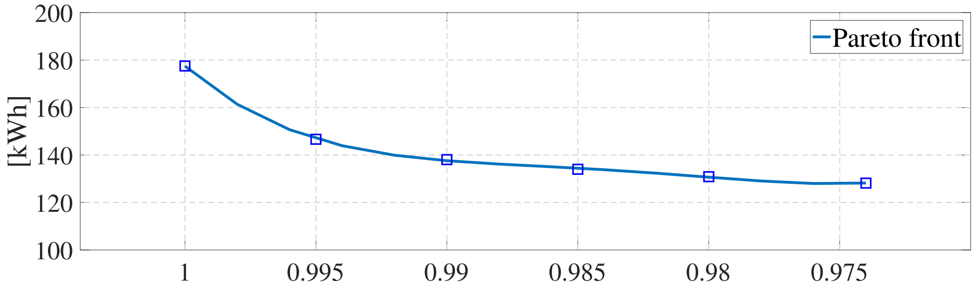

(c) Building B3.

Figure 13 – First scenario of study. Pareto Front regarding the relation between total HVAC+lighting ($E^T + E^I$) energy and minimum permissible comfort index ($\underline{C}_i$).

5 Second Scenario of Study: Buildings Operating in a Microgrid

The Second scenario of study considers multiple buildings operating in a microgrid. The proposed strategy (including the grid model) was tested in the 13-bus microgrid shown in Fig. 14, detailed information of branches impedance, current magnitude limits, among others can be found in the Appendix A. It is important to highlight that in this work it is only considered the case in which the microgrid operates connected to the main grid, islanded operation is not studied. The three buildings analyzed in the First scenario of study were duplicated and located in individual buses of the grid. Table 4 presents the buildings information, the index of each building represents the number of the bus where it is connected to the microgrid, e. g. B6 corresponds to the building located at bus 6.

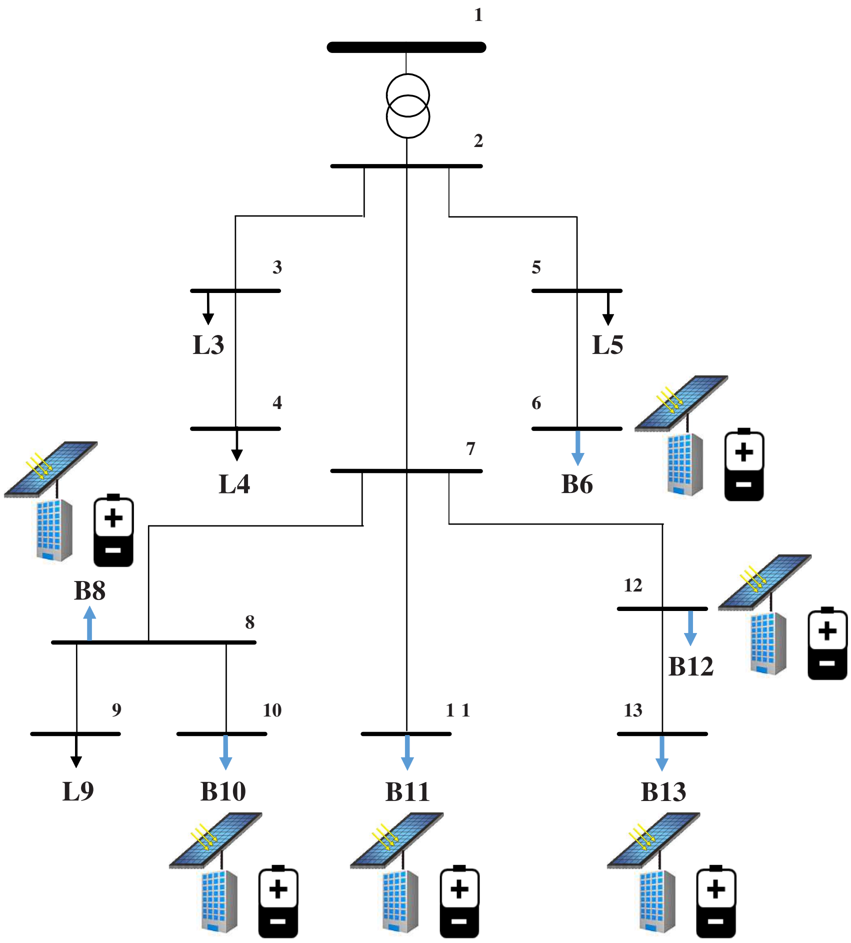

Figure 14 – Microgrid test case, L represents non-manageable loads and B represents buildings.

Table 4 – Second scenario of study. Buildings general information.

	B6 / B11	B8 / B12	B10 / B13	Units
Usage	Classrooms	Technology	Offices	—
Operating time	[7:00-21:00]	[8:00-18:00]	[8:00-18:00]	—
A_{PV}	210	260	200	$[m^2]$
E^B	70	88	68	[kWh]
Zones	10	10	10	—

The non-manageable loads of the microgrid are depicted in Fig. 16. For all buildings, the minimum permissible comfort index was defined as $\underline{C}_i = 0.995$, while temperature and illuminance set points were subject to operate within $[20-25]^o$C and $[400-600]$Lx, respectively. The voltage thresholds of the microgrid $\underline{V}$ and $\overline{V}$ were defined as $0.93 * V^{NOM}$ and $1.05 * V^{NOM}$, regarding the Brazilian regulation [43]. Four cases were implemented, in cases IV and VI each building optimize its own operation in an individualist strategy, without considering the grid or other buildings. Initially, the optimal solution for each building is found following the strategy used in the First scenario of study, minimizing the cost of each building operation. Later, the demand of each building is defined as parameter and the MILP model (including the electrical grid model) is solved to obtain the operation of the microgrid. Notice that, for theses cases the operation of the microgrid is not optimized, the solution of the MILP model represent just the solution of a common power flow problem. In cases V and VII the microgrid central operator coordinates the buildings and microgrid operation. In these cases, the problem is solved following the entire proposed strategy, executing the pre-processing stage for each building and solving the MILP model considering buildings and electrical grid together in the modeling to minimize the total cost of the energy imported from the main utility at bus 1.

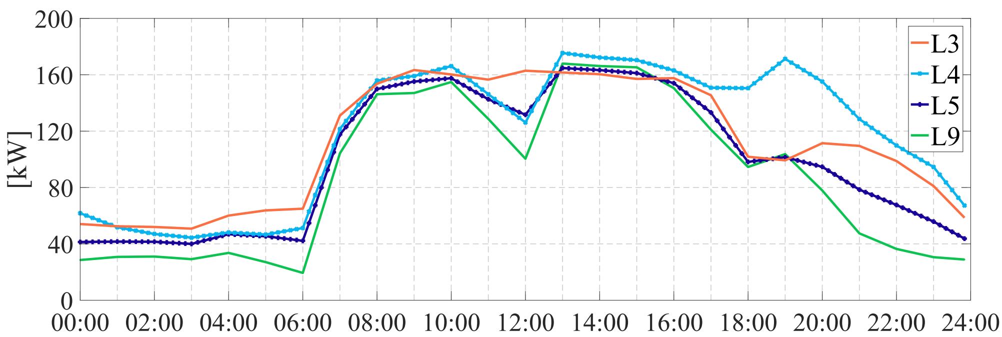

Figure 15 – Non-manageable loads of the microgrid.

The cases analyzed in the Second scenario of study can be described as,

Case IV: Only consumption management, individualist scheme,
Case V: Only consumption management, centralized scheme,
Case VI: Consumption management, PV, ESS, individualist scheme,
Case VII: Consumption management, PV, ESS, centralized scheme.

The problem to be solved for cases V and VII can be described as,

$$\min \quad (2.39),$$

subject to: (2.1)–(2.2) , (2.3), (2.4), (2.7)–(2.11), (2.17), (2.12)–(2.14), (2.18)–(2.23), (2.24), (2.28)–(2.32), (2.33)–(2.35), (2.37)–(2.38), (3.1)–(3.4), (3.5), (3.6)–(3.11), (3.23)–(3.22), (3.25)–(3.27), (3.28)–(3.38), (3.39).

5.1 Buildings Consumption Management Capacity

Cases IV and V do not include PV and ESS into the analysis in order to study the relation between the buildings consumption management capacity and grid operation. As shown in Fig. 16, in Case IV, which considered buildings optimizing their operation individually, between 14:00-15:00h, the voltage magnitude at bus 9 is below the minimum limit. This event coincides with the peak power consumption period, as presented in Fig. 17 for case IV. In contrast, in Case V, the voltage profile in Fig. 16 is improved due the action executed by the central operator, coordinating the BEMS of all buildings. As presented in Fig. 17, the buildings demand and power losses are reduced between 14:00-15:00h, allowing the central operator to meet the microgrid voltage constraint. In total, buildings demand and power losses decreased (in average) 8.5% during this period.

In Case V, the coordinated action of BEMSs is based on the management of HVAC units and lighting appliances. To show this, Fig. 18 presents the temperature and illuminance level set points of zone 1 of building B10. For Case V, the HVAC unit is activated at 13:50h (before the zone starts to be occupied at 14:00h), with the minimum temperature (20^{o}C) to pre-cool the zone, leveraging the mass volume inertia to storage cooling energy. Additionally, between 14:00-15:00h, temperature is defined to the maximum value (25^{o}C), while the illuminance level is reduced. Most of the zones in all the buildings operate in a similar fashion during the same time period. As a consequence, during this period the power demand of buildings B6, B8, B10 decreased (in average) 6%, 10.3% and 11.1%, respectively, when comparing with Case IV; buildings B11, B12 and B13 described similar results. This strategy allows the central operator to meet the microgrid voltage constraint.

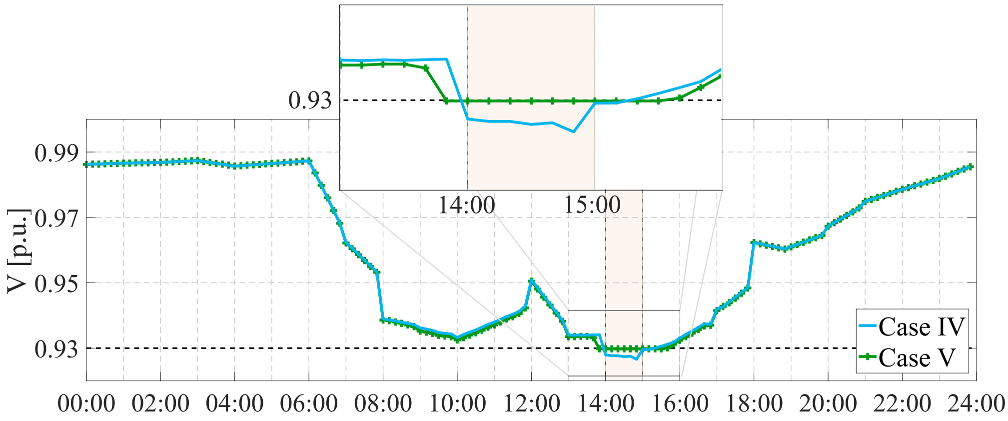

Figure 16 – Second scenario of study. Voltage at bus 9. Cases IV and V.

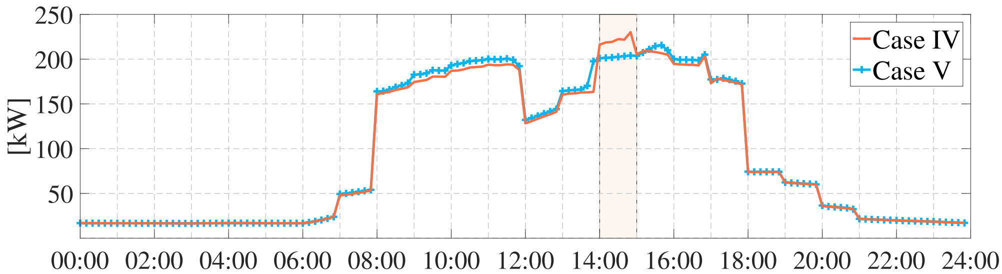

Figure 17 – Second scenario of study. Buildings demand and power losses. Cases IV and V.

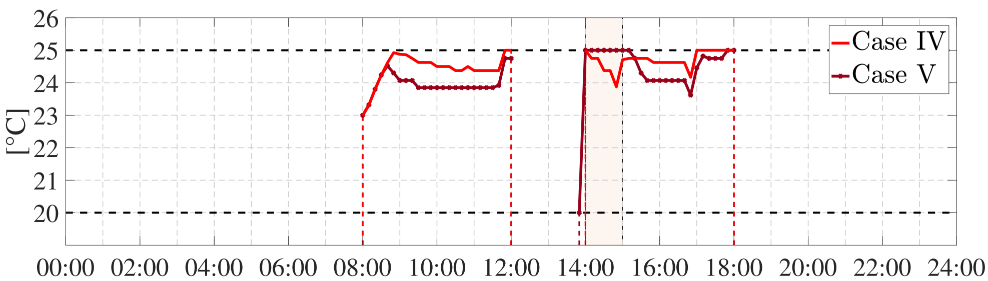

(a) Temperature set point.

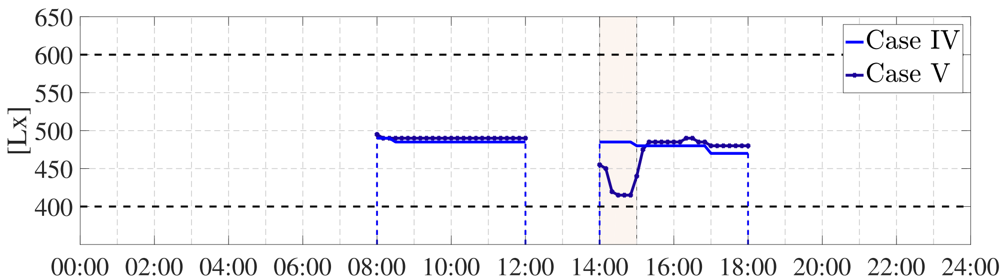

(b) Illuminance level set point.

Figure 18 – Second scenario of study. Temperature and illuminance set points, zone 1 of Building B10 during the occupied periods. Cases IV and V.

Notice in Fig. 18 for Case V, that during the time periods before 14:00h and after 15:00h, the HVAC units operate with lower temperature values and the lighting appliances with higher illuminance level, when compared with Case IV. As a consequence, the power consumption of the buildings is increased, as can be seen in Fig. 19. The rationale behind these management decisions is to meet the comfort constraint at the end of the total horizon. In total, the total energy consumption in Case V is 1.3% higher than in Case IV. Nevertheless, in Case IV the voltage constraint is not guaranteed. A general comparison of both cases is presented in Table 5.

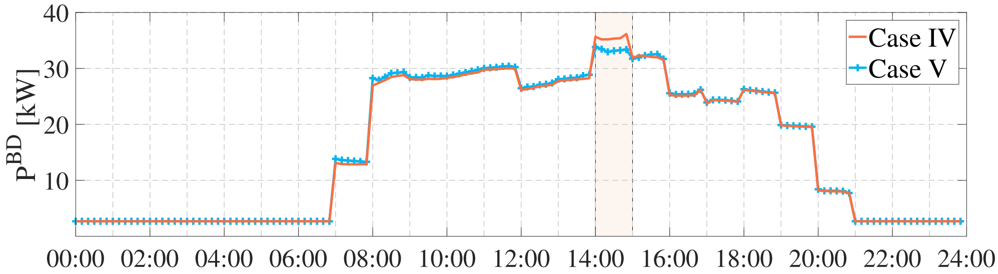

(a) Building B6.

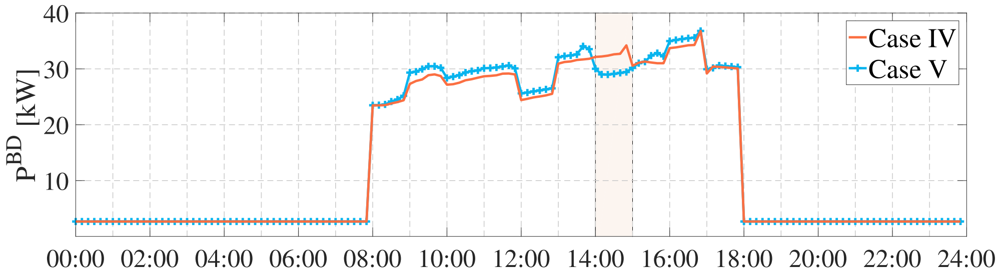

(b) Building B8.

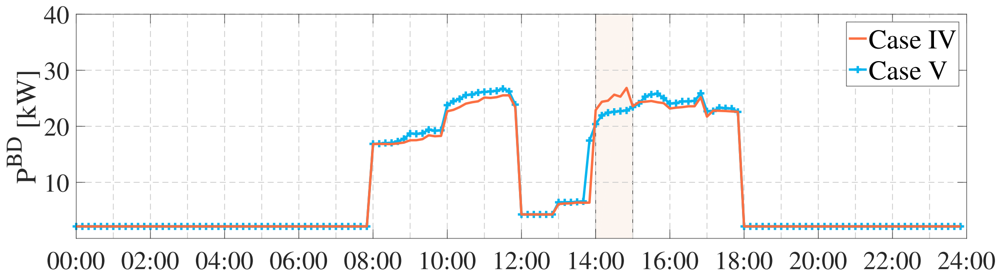

(c) Building B10.

Figure 19 – Second scenario of study. Buildings power consumption. Cases IV and V.

Table 5 – Second scenario of study. Comparison results for cases IV and V ($\underline{C}_i = 0.995$).

	Case IV	Case V
Consumption [kWh]	2217.7	2246.7
Total Cost [$]	579.5	586.8
Peak power [kW]	230.1	215.6
V [p.u]	0.926	0.930

Table 6 – Second scenario of study. Case V with different values of $\underline{C}_i$.

$\underline{C}_i$	1	0.995	0.900
Consumption [kWh]	2466.8	2246.7	2060.3
Total Cost [$]	645.8	586.8	540.6
Peak power [kW]	247.6	215.6	201.72
V [p.u]	0.926	0.930	0.930

As mentioned before, the comfort constraint plays an important role in the management decisions. Table 6 presents a comparison of the microgrid operation when the minimum permissible comfort index in buildings is modified. If the constraint is relaxed to $\underline{C}_i = 0.90$, a solution with a total cost 7.8% lower than the base case ($\underline{C}_i = 0.995$), can be obtained. On the other hand, and depending on the conditions, if the management capability is limited ($\underline{C}_i = 1$), a high cost and technically unfeasible solution (voltage limits violation) is obtained.

5.2 Buildings Operation with PV and ESS

Fig. 20 depicts the voltage magnitude profile at bus 9 for cases VI and VII. In both cases, the microgrid operates within the voltage magnitude limits. As can be seen in Fig. 21, the buildings demand and power losses decreased due that PV generation is available, supplying locally the consumption of buildings. Additionally, as was expected, during the medium/high price period from 15:00h to 21:00h, in both cases the ESS operates in discharging mode, supplying locally a portion of the buildings consumption as well. Moreover, in Case VII the buildings demand and power losses are reduced in the morning, between 8:00h and 12:00h. This result is not related to the management of HVAC and lighting appliances but instead to the ESS operation. To see this, observe in Fig. 22, that in Case VII the charging operation of the ESS in buildings B6, B8 and B10 is completely shifted to early in the morning. Buildings B11, B12, B13 described similar results. This coordinated action reduce the power peak of the buildings demand and power losses by 15.3% in Case VII, when compared with Case VI, additional results are presented in Table 7.

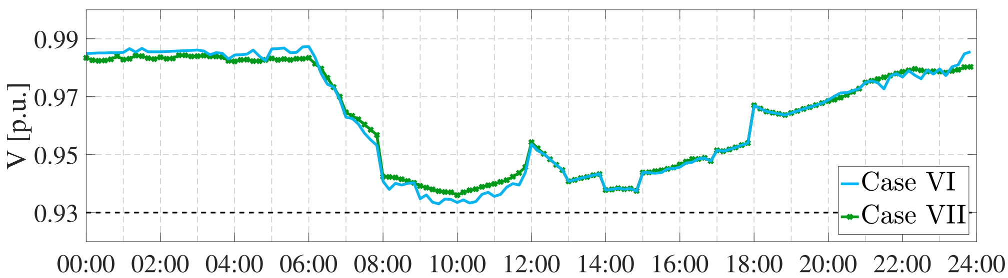

Figure 20 – Second scenario of study. Voltage at bus 9. Cases VI and VII.

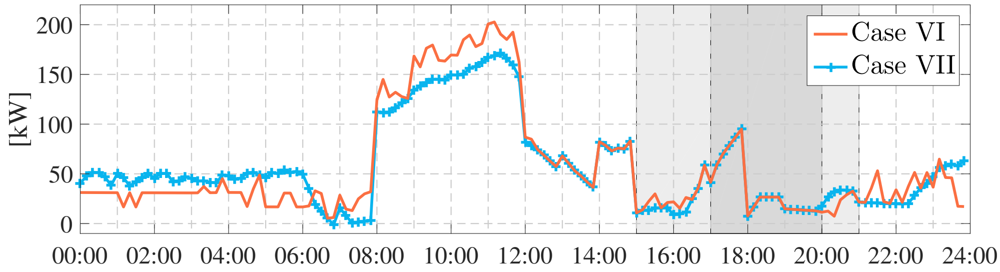

(a) Buildings demand and power losses.

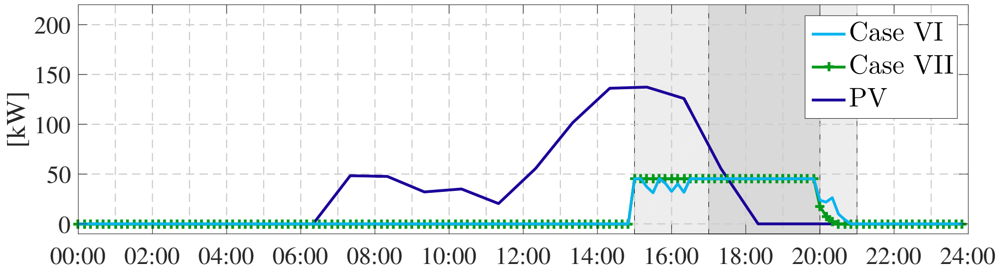

(b) Local power generation.

Figure 21 – Second scenario of study. Microgrid demand and generation. Cases VI and VII.

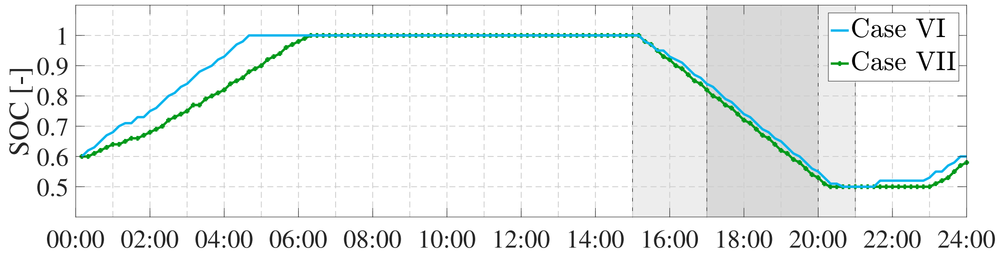

(a) Building B6.

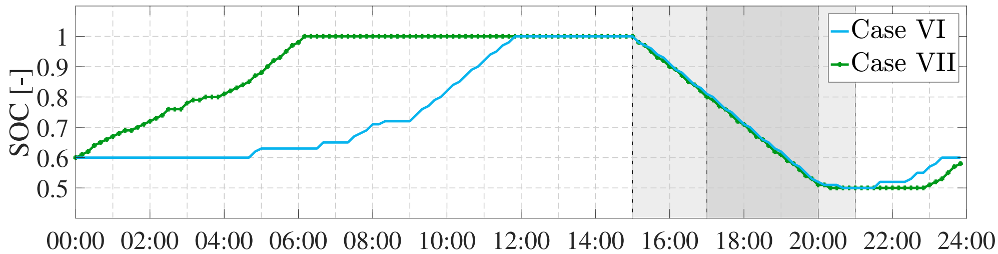

(b) Building B8.

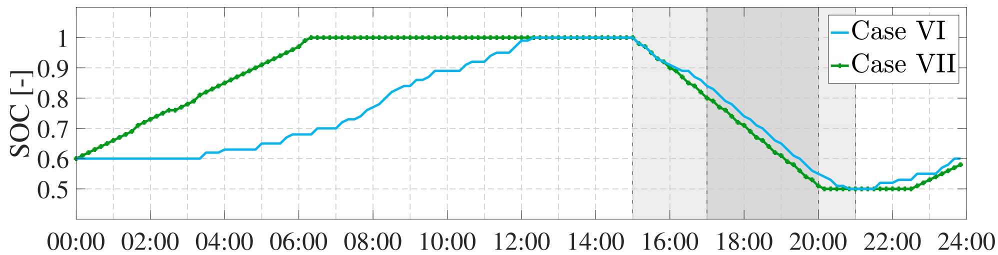

(c) Building B10.

Figure 22 – Second scenario of study. SOC of the ESS. Cases VI and VII.

Table 7 – Second scenario of study. Comparison results for cases VI and VII ($\underline{C}_i = 0.995$).

	Case VI	Case VII
Consumption [kWh]	1368.4	1362.7
Total Cost [$]	321.1	319.8
Peak power [kW]	202.7	171.8
V [p.u]	0.933	0.936

Since PV and ESS systems supply locally the buildings demand, the operation of the internal manageable appliances (HVAC and lighting) is not modify to avoid the voltage limit violations. Thus, internal appliances operate at the optimal point found individually, without modifying their consumption to respond to microgrid technical needs. As presented in Fig. 23, the power consumption related to HVAC, lighting and non-manageable devices is equivalent in both cases.

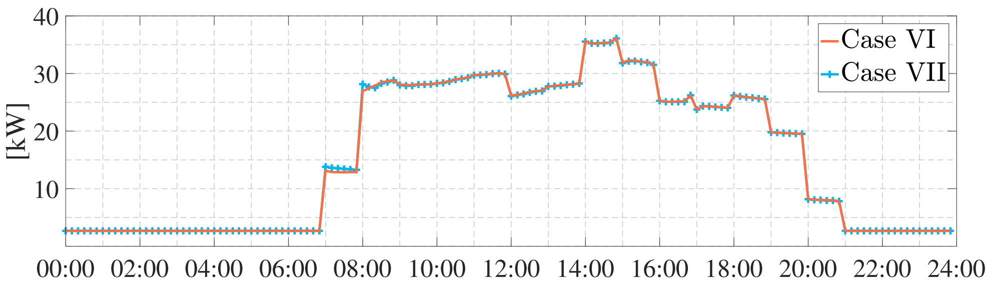

(a) Building B6.

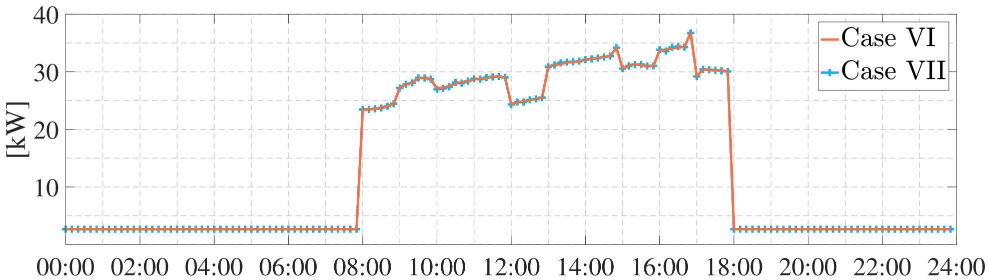

(b) Building B8.

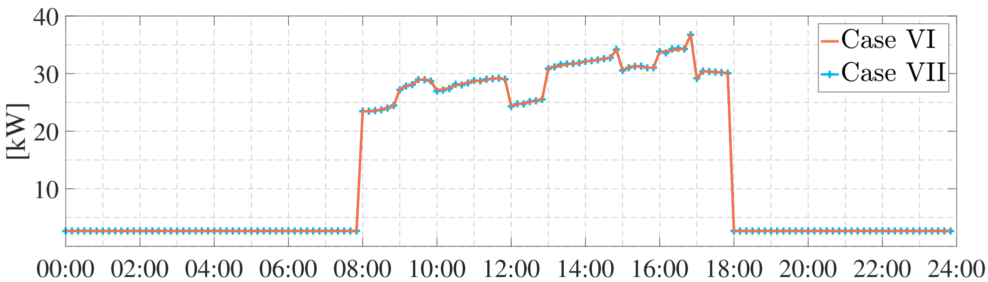

(c) Building B10.

Figure 23 – Second scenario of study. Buildings power consumption. Cases VI and VII.

5.2.1 Processing Time and Performance of the Proposed Strategy

In general, the pre-processing stage of a single building was executed in 24s, approximately. It is important to remind this stage is executed in advance, before the beginning of the time horizon. Regarding Case VI, in which the operation of each building was optimized considering consumption management, PV and ESS, the maximum processing time of the optimization stage for a single building was 7s. As for Case VII, considering that the microgrid operator solves the entire problem in a centralized fashion, the pre-processing stage of the six buildings was executed in 144s, while the processing time of the optimization stage was about 250s.

On the other hand, with the aim of assessing the error of the proposed approach, the validation process described in Fig. 24 was developed. The optimal operation of each building was simulated in EnergyPlus using the values of $T_{i,z,t}$, $I_{i,z,t}$ and $u_{i,z,t}$ obtained by applying the proposed strategy. This simulation allowed obtaining the consumption profile of each building, specially the consumption of HVAC units. Using these demand profiles and the scheduled of the ESS as parameters, the microgrid operation was estimated solving the non-linear power flow formulation in Sec.2.3.1, using AMPL and the solver tool IPOPT [44]. According to this, the maximum error for all buildings was near to 4.5% when comparing the individual power consumption obtained with the MILP model and EnergyPlus. Additionally, an error of 1.5% was observed for the total cost of the energy imported by the microgrid from the main utility, when comparing the solution of the MILP model with the results of the non-linear power flow formulation.

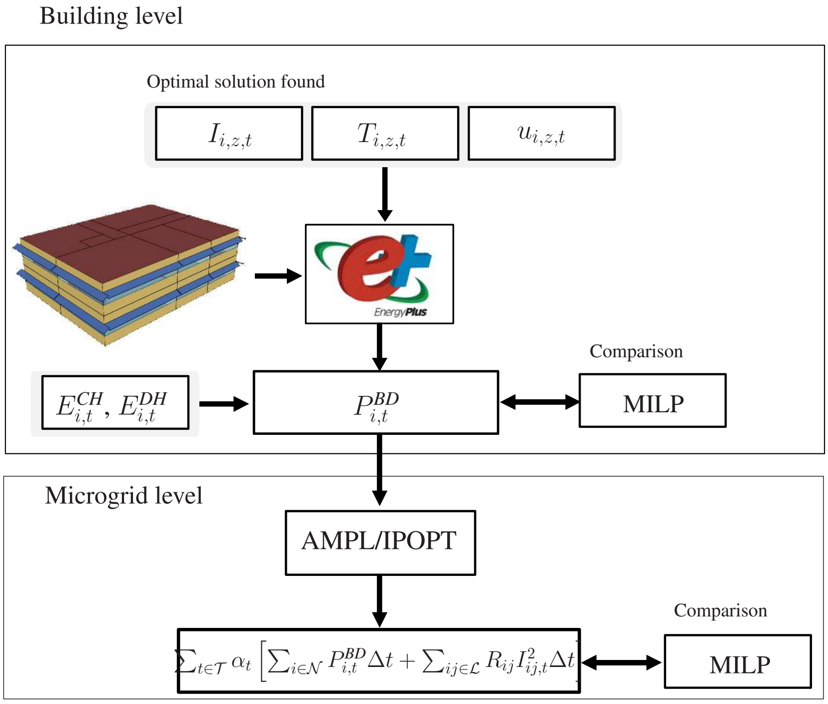

Figure 24 – Proposed validation strategy.

Finally, capturing the thermal dynamics of zones is one of the main issues to model the operation of buildings satisfactorily. In order to asses the capability of the proposed strategy to capture this phenomena, a comparison between the results of the MILP model and the simulation executed according to Fig. 24 was conducted. Fig. 25 shows the temperature of three zones with different occupancy profiles. The temperature obtained by the MILP model and the results from EnergyPlus are equivalent for all the zones; some differences are observed at the moments when the state of the zone changes (Occupancy), although along the total time horizon the MILP model captures the thermal dynamics satisfactorily. In fact, the maximum error obtained for the temperature of all buildings zones was 2.1%.

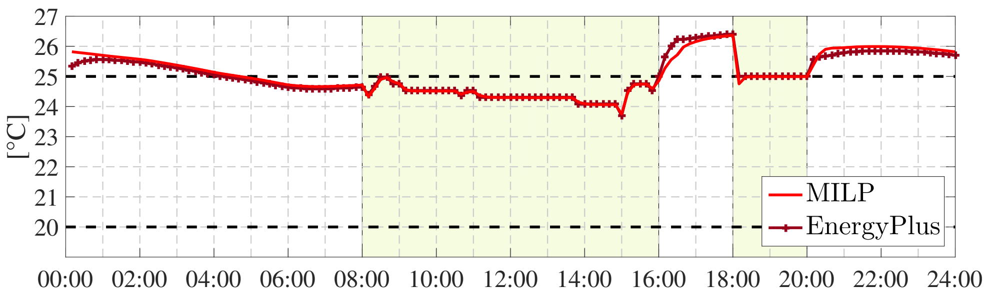

(a) Zone 8 of building B6.

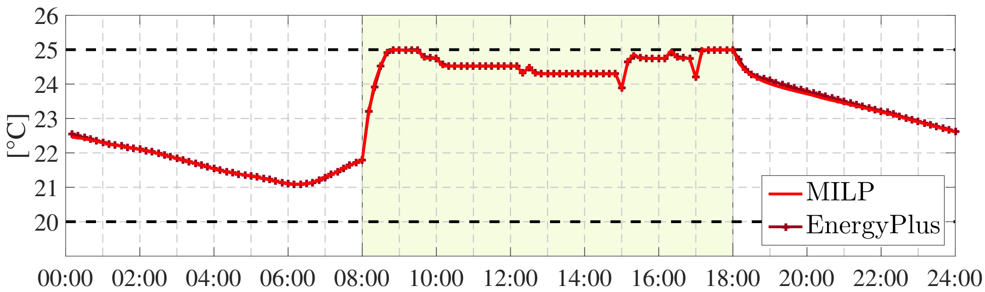

(b) Zone 6 of building B8.

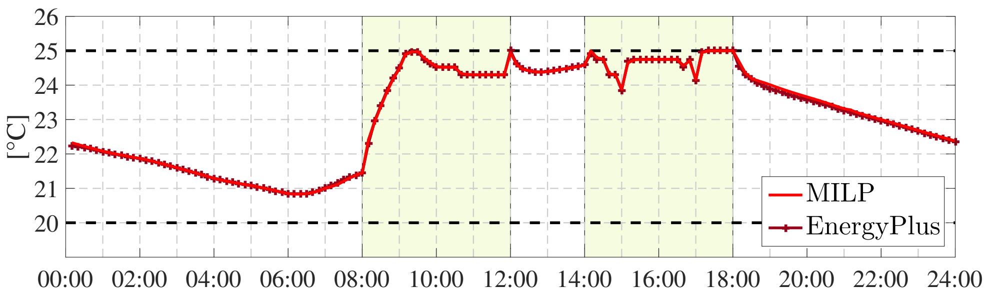

(c) Zone 2 of building B10.

Figure 25 – Second scenario of study. Zones temperature regarding MILP model and EnergyPlus simulations.

6 Third Scenario of Study: Addressing Uncertainty through a Rolling Horizon Scheme

The First and Second scenarios of study were analyzed with a deterministic approach, assuming that forecasted information described a perfect knowledge of real conditions. Nevertheless, defining the operation at the beginning of the time horizon limits the capability of buildings and the microgrid to react to unexpected events or significant disturbances. Forecasting errors may bring out a sub-optimal operation.

Some strategies to address scheduling problems under uncertainty have been proposed [45–48]. In general, these approaches could be classified into proactive and reactive strategies [49]. Proactive schemes are based on the consideration of all possible cases, especially through stochastic programming. For instance, in [45], it is presented a stochastic model predictive control strategy for building climate control that takes into account the uncertainty of weather predictions; in [46], authors present a distributed approach based on a locational marginal price method integrating congestion free energy and reserve provision from buildings in distribution grids, considering uncertainties through a stochastic disturbance in the buildings load. However, the solution of proactive schemes may be too conservative, since the model must take into account all the possibilities even the ones that do not occur eventually [49]. In contrast, reactive approaches aim at modifying a schedule found using expected conditions, in order to adjust it to disturbances, modifications or updated system data; particularly, rolling horizon schemes belong to this category. In [47], an MILP based rolling optimization approach under real time pricing policy is introduced to manage energy consumption of a smart home equipped with ESS and PV systems; meanwhile in [48], an energy management system based in a rolling horizon strategy for a renewable-based microgrid is proposed. Thus, in this Chapter it is presented a rolling horizon scheme to address these issues. By updating at each time step forecasting information and measures of variables such as irradiance, occupancy and temperature of the zones, buildings and microgrid operation may be adjusted regarding to real conditions.

6.1 Rolling Horizon Scheme

The proposed RH scheme is presented in Fig. 26. The total horizon ($\mathcal{T} = 24h$) is divided into two periods: a short horizon, with length $T^S = 1h$ and discretized time steps of length $\Delta t^S = 10min$; and a long horizon, with length $T^L = 23h$ and time steps of length $\Delta t^L = 1h$. Following the proposed strategy in Fig. 26, the pre-procesing stage is executed in advance, before the beginning of the total horizon. At instant t the measures and forecasts of variables G_t, T_t^{OUT}, and $\kappa_{i,z,t}^{Oc}$ are updated. Additionally, $T_{i,z,t}$ and $I_{i,z,t}$ are measured in order to update the current state of buildings. Then, the optimization stage is executed and the solution found is implemented for the control stage (t^C), which corresponds to the first time step of the short horizon. At instant $t+\Delta t^S$, t^C and T^S are redefined and the problem is solved again. The scheme continues in the same fashion, updating the measures, forecasting information, t^C and T^S, to solve the problem at each time step. At instant T^S, the total window horizon is rolled Δt^L (In this case 1h) ahead, and t^C, T^S, T^L are redefined. This procedure is executed along the total horizon (24h); when the last time step of the total horizon (In this case at 23:50) is reached, a preliminary solution for the next day is already available. At this moment the pre-processing stage is executed again, in order to update the approximation of $f_{i,z,t}^{CCT}$, $f_{i,z,t}^{EIT}$, $f_{i,z,t}^{SHR}$, and $q_{i,z,t}^{Srf}$. Later, the RH scheme continues executing the procedure already described.

In this case, it is assumed the long horizon starts exactly at the beginning of the next hour due to considerable changes in building operation are characterized by occurring at these moments. For instance, offices buildings open at 08:00h, lunch time starts 12:00h and so forth. The main advantage of the proposed RH scheme is that the short length of Δt^S allows capturing significant variations in the time steps near to t^C; meanwhile, the large length of Δt^L reduces the amount of forecasting information required by the central operator. Particularly, using $T^S = 1h$, $\Delta t^S = 10min$, $T^L = 23h$ and $\Delta t^L = 1h$, each variable requires 28 forecasted values, in contrast to the 144 values (24h with 10min time steps) used by the deterministic approach in Case VII. Algorithm 6.1 summarizes the general procedure of the proposed RH scheme, additional variables such as the demand of the internal non-manageable appliances ($P_{i,t}^{BL}$), the electrical devices usage profile ($\kappa_{i,z,t}^{Ed}$), among others, can be measured to update the buildings state and enhance the RH approach.

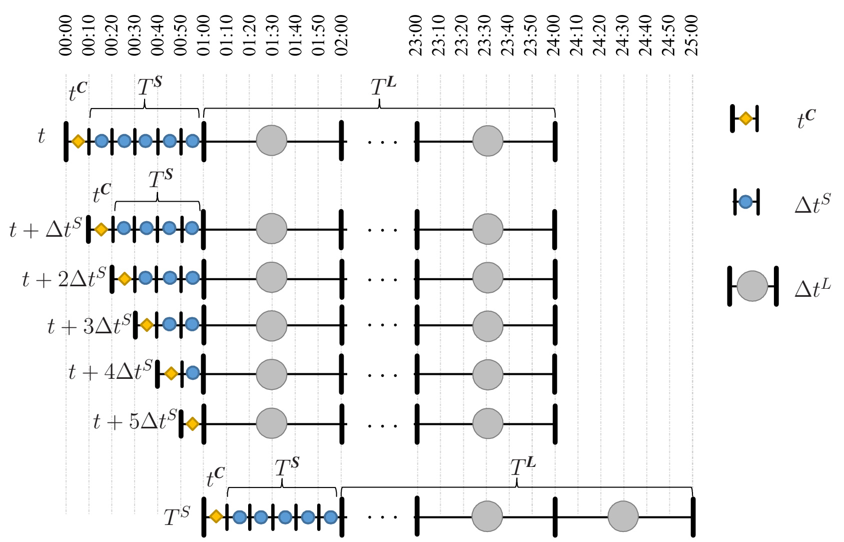

Figure 26 – Rolling horizon (RH) scheme. In cases VII-RH, total horizon is 24h, $\Delta t^S = 10$min and $\Delta t^L = 1$h.

Algorithm 6.1 Rolling Horizon Scheme

$s \leftarrow (T^S/\Delta t^S)$, $l \leftarrow (T^L/\Delta t^L)$
While: Executing RH
  Execute pre-processing stage
  for: $h = 0 : l$
    $T^L \leftarrow [h+1 : \Delta t^L : h+l]$
    for: $k = 1 : s$
      $t^C \leftarrow h + (k * \Delta t^S)$
      $T^S \leftarrow [t^C + \Delta t^S : \Delta t^S : h + s * \Delta t^S]$
      Update measures of G_t, T_t^{out}, $\kappa_{i,z,t}^{Oc}$, $T_{i,z,t}$, $I_{i,z,t}$
      Update forecasting data for the short horizon $\in T^S$
      Update forecasting data for the long horizon $\in T^L$
      Solve 2.39 for $t^C \cup T^S \cup T^L$
      $k \leftarrow k + 1$
    end
    $h \leftarrow h + 1$
  end
end

6.2 Third Scenario of Study

In order to assess the performance of the proposed RH scheme, in the Third scenario of study three cases were implemented. Cases VII-RH(a), VII-RH(b) and VII-RH(c) are equivalent to Case VII studied in the Second scenario, although each case uses different sets of forecasting information in order to analyze the effects of forecasting data errors on the final solution found by the proposed RH scheme. Fig. 27 presents the forecasts and measures of outdoor temperature T_t^{OUT} and irradiance G_t, the measures information corresponds to the data set used in Case VII. In Case VII-RH(a), the mean absolute percent difference between the forecasts and measures is 4.7% for the temperature and 44.4% for the irradiance. In Case VII-RH(b), these differences are 7.7% and 54.6%; while in Case VII-RH(c), they correspond to 7.7% and 104.5% for temperature and irradiance, respectively. On the other hand, the same set of information was used as forecasts and measures for $\kappa_{i,z,t}^{Oc}$. Since measures data of the indoor temperature $T_{i,z,t}$ is not available (due to it depends on the operation of the building), a strategy to emulate these measures was developed. After solving the problem in the optimization stage at each time step, the solution of each building was simulated in EnergyPlus, the values obtained for the zones temperature corresponding to the specific time step being analyzed were defined as the measures of $T_{i,z,t}$. As for the illuminance level $I_{i,z,t}$, it was considered the natural illuminance component $I_{i,z,t}^{OUT} = 0$, thus, the measures of $I_{i,z,t}$ corresponds to the same value found during the optimization stage.

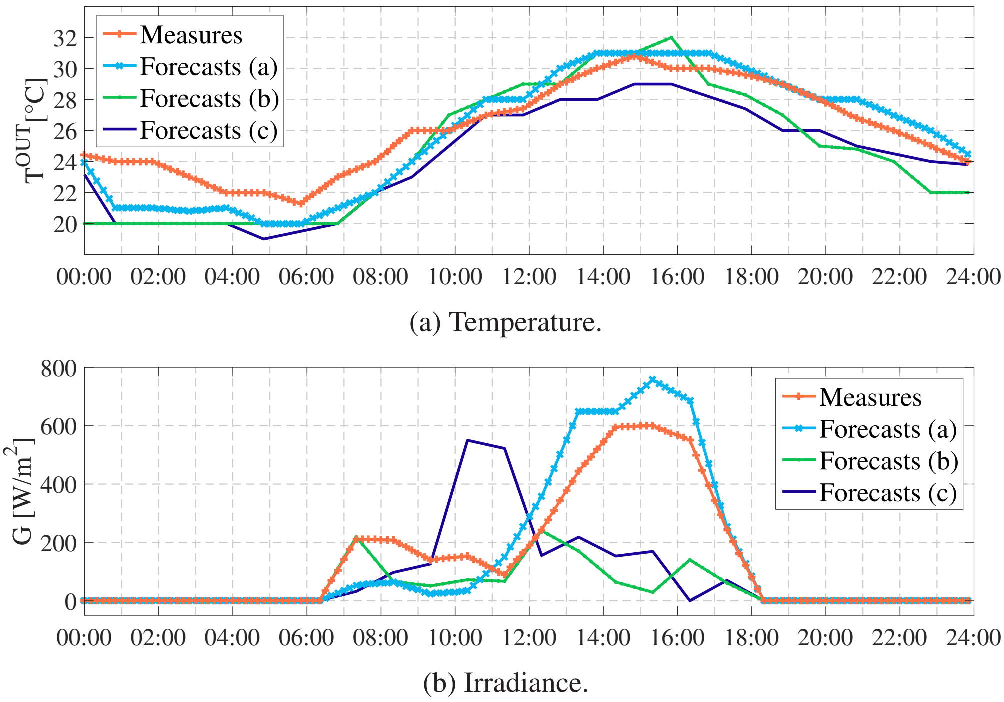

Figure 27 – Third scenario of study. Measures and forecasts of weather conditions. Cases VII-RH(a)-(c).

As can be observed in Fig. 28, the microgrid operation in cases VII-RH(a)-(c) is equivalent to the optimal solution found in Case VII, which assumed perfect knowledge of the real conditions. The nature of the RH scheme does not allow modeling the constraint (2.9) related to the final state of charge of the ESS, since the end of the total horizon is rolled during the optimization. This is, meanwhile in Case VII the central operator must guarantee a $SOC_{i,t}$ (in this particular case 0.6) at the end of the day, in cases VII-RH(a)-(c) only the minimum $\underline{SOC}_{i,t}$ can be guaranteed. This characteristic explains the differences between cases VII and VII-RH(a)-(c) in the buildings demand and power losses at the end of the day in Fig. 28. As can be observed in Fig. 29, for Case VII-RH(a), the ESS systems of buildings B6, B8 and B10 are not re-charged at the end of the day, the $SOC_{i,t}$ stays near to $\underline{SOC}_{i,t}$ instead. This behavior represents a reduction in the amount of energy imported from the utility. As a consequence the total cost of the solutions found through the proposed RH scheme differs of the total cost obtained by the deterministic approach. In fact, in cases VII-RH(a)-(c), the total cost differs by 3.8%, 3.9% and 5.7% from the total cost of Case VII.

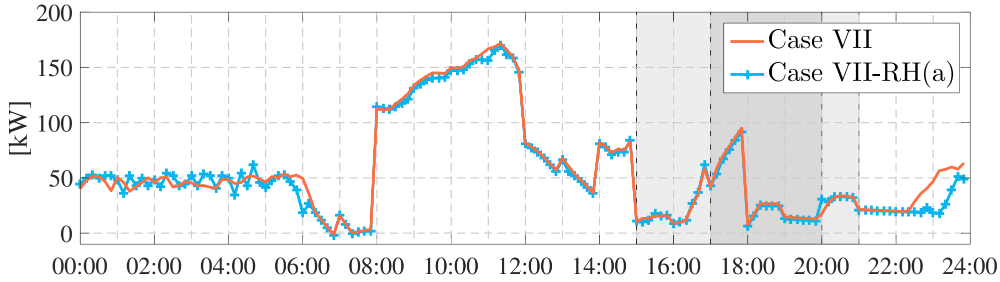

(a) Case VII-RH(a).

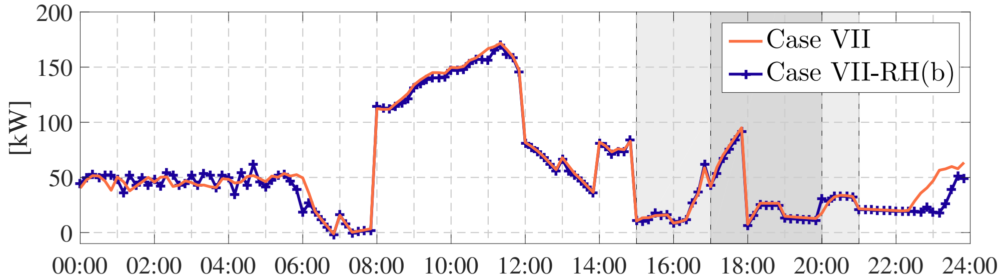

(b) Case VII-RH(b).

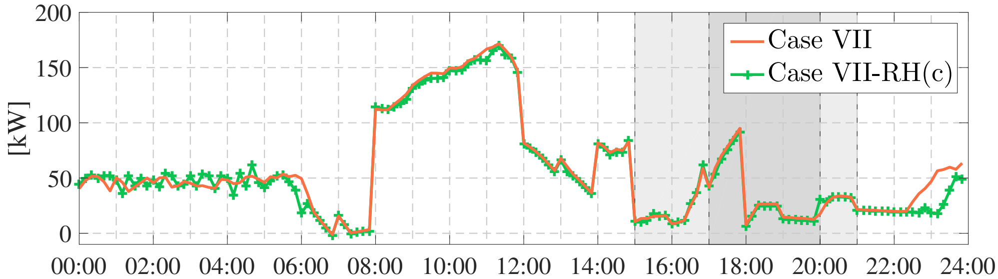

(c) Case VII-RH(c).

Figure 28 – Third scenario of study. Buildings demand and power losses. Cases VII-RH(a)-(c).

Table 8 – Third scenario of study. Comparison results for cases VII and VII-RH(a)-(c).

	Case VII	Case VII-RH(a)	Case VII-RH(b)	Case VII-RH(c)
Consumption [kWh]	1362.7	1311.0	1307.5	1289.6
Total Cost [$]	319.8	307.7	307.5	301.6
Peak power [kW]	171.8	170.2	169.8	170.6
V [p.u]	0.936	0.936	0.936	0.936

On the other hand, comparing the operation of the internal appliances of buildings in Fig. 30, for Case VII-RH(a) the demand profiles of buildings B6, B8 and B10 were equivalent to the profiles obtained in Case VII. In fact, the mean absolute percent difference in this case was 0.8%, 0.4% and 0.3% for these buildings. Similar results were obtained for all the buildings in cases VII-RH(b)-(c). These results show the capacity of the proposed RH scheme to follow the real conditions and optimize the operation of buildings regarding them. Table 8 presents additional results.

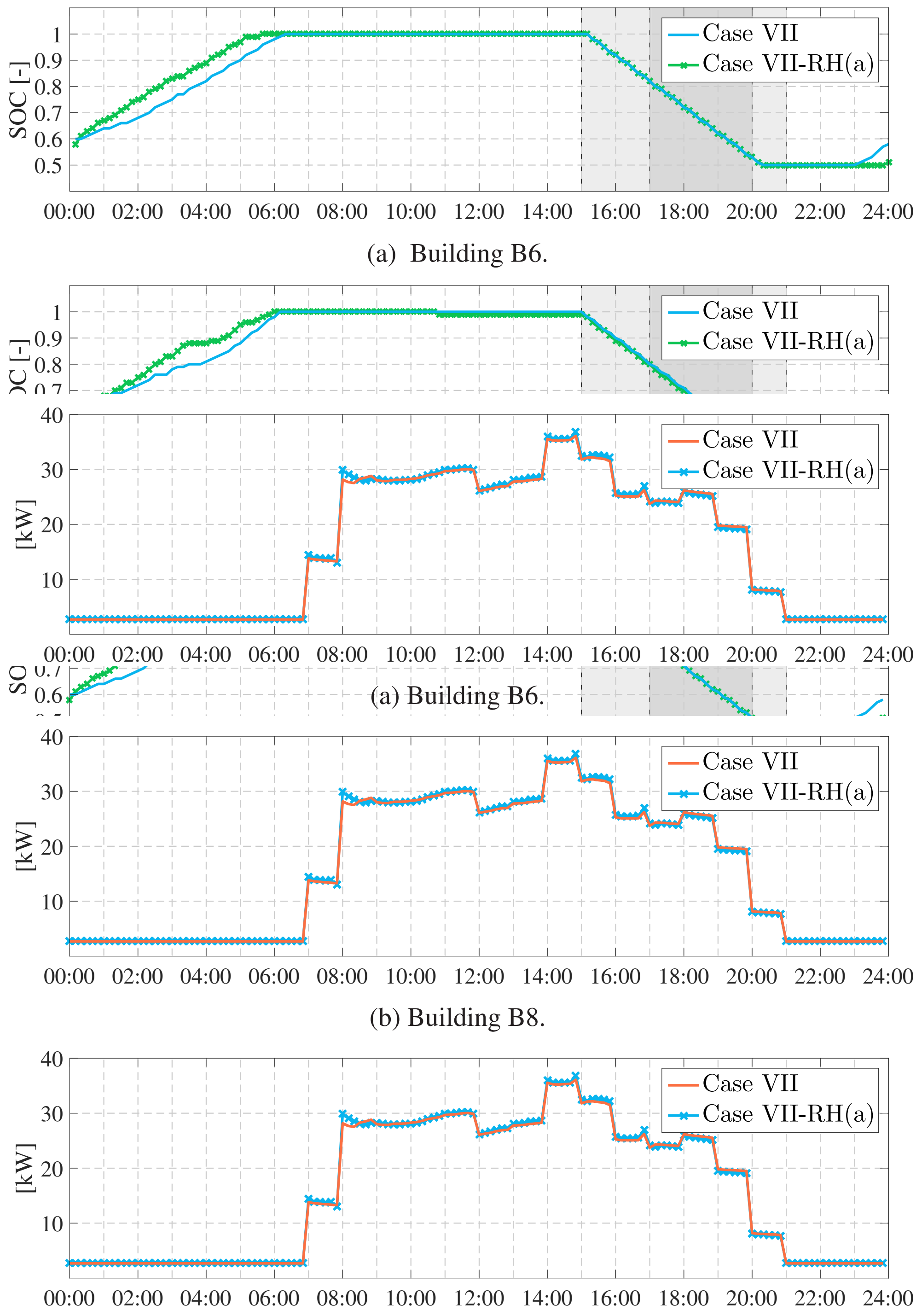

(a) Building B6.

(a) Building B6.

(b) Building B8.

(c) Building B10.

Figure 30 – Third scenario of study. Buildings power consumption. Cases VII and VII-RH(a).

Finally, the mean processing time of the optimization stage to solve the problem for the total horizon in cases VII-RH(a)-(c) was approximately 50s (at each time step), in contrast to the 250s required to solve the problem with discretized time steps for the total horizon with the deterministic approach in Case VII.

Conclusion

- A detailed MINLP model to coordinate, in a centralized fashion, the operation of multiple buildings in a microgrid, was presented. Additionally, a strategy that simplifies the original model was proposed, based on a set of linearization techniques and equivalent representations, obtained through a pre-processing stage executed in EnergyPlus;

- Modifying the typical strategy of buildings operation, which considers fixed set points for the HVAC units and lighting appliances, allows managing the consumption in order to minimize the total cost and producing a demand respond to the dynamics of the energy price;

- According to the results, including the electrical grid operation in the buildings management problem allows taking advantage of the buildings management capacity to enhance the electrical grid operation, while technical constraints at building level such as comfortable conditions for the occupants are ensured;

- Acceptable errors were obtained when comparing the proposed strategy with the original formulation. Also, low processing time was obtained since the proposed strategy does not use multiple simulations during the optimization stage. On the other hand, the results of the Third scenario of study show the capability of the proposed RH strategy to adjust the buildings operation and follow the real conditions, finding solutions equivalents to the optimal solution found with a deterministic approach. Additionally, the RH scheme performs low processing time as well. These features can make it suitable for future real time implementations.

Future Work

- Including a mathematical representation of electrical vehicles as part of the buildings loads;

- Testing the proposed strategy in large-sized buildings with more than 10 zones and larger microgrids, in order to study the processing time and computing requirements;

- Developing the EnergyPlus model of a real building to test the proposed strategy regarding real information;

- Developing a more detailed uncertainty assessment study of the proposed RH scheme. This can be done using a Monte-Carlo Simulation framework.

Publications

The publications resulting directly from this research work are shown below:

- J. A. Pinzon, P. P. Vergara, L. C. P. da Silva, and M. J. Rider, "An MILP Model for Optimal Management of Energy Consumption and Comfort in Smart Buildings," in 2017 IEEE Power Energy Society Innovative Smart Grid Technologies Conference (ISGT), April 2017, pp. 1–5.

References

[1] N. Liu, Q. Chen, J. Liu, X. Lu, P. Li, J. Lei, and J. Zhang, “A heuristic operation strategy for commercial building microgrids containing evs and pv system,” *IEEE Trans. Ind. Electron.*, vol. 62, no. 4, pp. 2560–2570, Apr. 2015.

[2] D. Kolokotsa, “The role of smart grids in the building sector,” *Energy and Buildings*, vol. 116, no. 15, pp. 703 – 708, Mar. 2016.

[3] A. Ghalebani and T. K. Das, “Design of financial incentive programs to promote net zero energy buildings,” *IEEE Trans. Power Syst.*, vol. 32, no. 1, pp. 75–84, Jan. 2017.

[4] PROCEL INFO, “Relatório completo da pesquisa de posse de equipamentos e hábitos de uso - classe residencial,” Rio de Janeiro, Jul. 2007.

[5] ——, “Relatório executivo da pesquisa de posse de equipamentos e hábitos de uso - classe comercial - AT,” Rio de Janeiro, Aug. 2008.

[6] Ministério da Ciência Tecnologia e Inovação and Joint Research Centre, “Redes elétricas inteligentes, diálogo setorial brasil-união europeia,” Brasília, Nov. 2014.

[7] PROCEL INFO, “Relatório completo da pesquisa de posse de equipamentos e hábitos de uso - classe comercial - AT,” Rio de Janeiro, Set. 2008.

[8] H. Hao, C. D. Corbin, K. Kalsi, and R. G. Pratt, “Transactive control of commercial buildings for demand response,” *IEEE Trans. Power Syst.*, vol. 32, no. 1, pp. 774–783, Jan. 2017.

[9] Z. Xu, X. Guan, Q. S. Jia, J. Wu, D. Wang, and S. Chen, “Performance analysis and comparison on energy storage devices for smart building energy management,” *IEEE Trans. Smart Grid*, vol. 3, no. 4, pp. 2136–2147, Dec. 2012.

[10] N. Wang, F. Fang, and M. Feng, “Multi-objective optimal analysis of comfort and energy management for intelligent buildings,” in *The 26th Chinese Control and Decision Conference (2014 CCDC)*, May 2014, pp. 2783–2788.

[11] T. Samad, E. Koch, and P. Stluka, “Automated demand response for smart buildings and microgrids: The state of the practice and research challenges,” *Proc. IEEE*, vol. 104, no. 4, pp. 726–744, Apr. 2016.

[12] F. Rahimi and A. Ipakchi, “Using a transactive energy framework: Providing grid services from smart buildings,” *IEEE Electrific. Mag.*, vol. 4, no. 4, pp. 23–29, Dec. 2016.

[13] D. Minoli, K. Sohraby, and B. Occhiogrosso, "IoT considerations, requirements, and architectures for smart buildings - energy optimization and next-generation building management systems," *IEEE Internet of Things Journal*, vol. 4, no. 1, pp. 269–283, Feb. 2017.

[14] E. Biyik, S. Genc, and J. D. Brooks, "Model predictive building thermostatic controls of small-to-medium commercial buildings for optimal peak load reduction incorporating dynamic human comfort models: Algorithm and implementation," in *2014 IEEE Conference on Control Applications (CCA)*, Oct. 2014, pp. 2009–2015.

[15] H. Zhao, D. Quach, S. Wang, H. Wang, H. Chen, X. Li, and S. X. D. Tan, "Learning based compact thermal modeling for energy-efficient smart building management," in *2015 IEEE/ACM International Conference on Computer-Aided Design (ICCAD)*, Nov. 2015, pp. 450–456.

[16] W. Liu, H. Wang, H. Zhao, S. Wang, H. Chen, Y. Fu, J. Ma, X. Li, and S. X. D. Tan, "Thermal modeling for energy-efficient smart building with advanced overfitting mitigation technique," in *2016 21st Asia and South Pacific Design Automation Conference (ASP-DAC)*, Jan 2016, pp. 417–422.

[17] J. Figueiredo and J. Martins, "Energy production system management - renewable energy power supply integration with building automation system," *Energy Convers. and Manage.*, vol. 51, no. 6, pp. 1120 – 1126, Jun. 2010.

[18] T. Cui, S. Chen, Y. Wang, Q. Zhu, S. Nazarian, and M. Pedram, "Optimal co-scheduling of hvac control and battery management for energy-efficient buildings considering state-of-health degradation," in *2016 21st Asia and South Pacific Design Automation Conference (ASP-DAC)*, Jan. 2016, pp. 775–780.

[19] M. K. Muthalib and C. O. Nwankpa, "Physically based building load model for electric grid operation and planning," *IEEE Trans. Smart Grid*, vol. 8, no. 1, pp. 169–177, Jan. 2017.

[20] S. Hanif, T. Massier, H. B. Gooi, T. Hamacher, and T. Reindl, "Cost optimal integration of flexible buildings in congested distribution grids," *IEEE Trans. Power Syst.*, vol. 32, no. 3, pp. 2254–2266, May 2017.

[21] D. Sturzenegger, D. Gyalistras, M. Morari, and R. S. Smith, "Model predictive climate control of a Swiss office building: Implementation, results, and cost-benefit analysis," *IEEE Trans. Control Syst. Technol.*, vol. 24, no. 1, pp. 1–12, Jan. 2016.

[22] A. A. Aizpuru, "Energy production and consumption scheduling in smart buildings," Master's thesis, School of Energy, Environment and Agryfood, Cranfield Univ., Cranfield, UK, 2016.

[23] C. D. Korkas, S. Baldi, I. Michailidis, and E. B. Kosmatopoulos, “Occupancy-based demand response and thermal comfort optimization in microgrids with renewable energy sources and energy storage,” *Applied Energy*, vol. 163, no. 1, pp. 93 – 104, Feb. 2016.

[24] S. Baldi, A. Karagevrekis, I. T. Michailidis, and E. B. Kosmatopoulos, “Joint energy demand and thermal comfort optimization in photovoltaic-equipped interconnected microgrids,” *Energy Convers. Manage.*, vol. 101, no. 1, pp. 352 – 363, Sep. 2015.

[25] R. Bălan, J. Cooper, K.-M. Chao, S. Stan, and R. Donca, “Parameter identification and model based predictive control of temperature inside a house,” *Energy and Buildings*, vol. 43, no. 2-3, pp. 748 – 758, Feb. 2011.

[26] L. H. Macedo, J. F. Franco, M. J. Rider, and R. Romero, “Optimal operation of distribution networks considering energy storage devices,” *IEEE Trans. Smart Grid*, vol. 6, no. 6, pp. 2825–2836, Nov. 2015.

[27] ASHRAE, *ASHRAE Handbook: Fundamentals*, Std., 2001.

[28] U.S. Department of Energy, *EnergyPlus Documentation, Engineering Reference-The Reference to EnergyPlus Calculations*, 2015.

[29] M. D. Knudsen and S. Rotger-Griful, “Combined price and event-based demand response using two-stage model predictive control,” in *2015 IEEE International Conference on Smart Grid Communications (SmartGridComm)*, Nov. 2015, pp. 344–349.

[30] J. Y. Joo and M. D. Ilić, “An information exchange framework utilizing smart buildings for efficient microgrid operation,” *Proc. IEEE*, vol. 104, no. 4, pp. 858–864, Apr. 2016.

[31] B. Verbruggen and J. Driesen, “Grid impact indicators for active building simulations,” *IEEE Trans. Sustain. Energy*, vol. 6, no. 1, pp. 43–50, Jan. 2015.

[32] G. R. Bharati, M. Razmara, S. Paudyal, M. Shahbakhti, and R. D. Robinett, “Hierarchical optimization framework for demand dispatch in building-grid systems,” in *2016 IEEE Power and Energy Society General Meeting (PESGM)*, Jul. 2016, pp. 1–5.

[33] U.S. Department of Energy. (2017, Oct.) Energyplus. [Online]. Available: https://energyplus.net/

[34] D. Pan, D. Wang, J. Cao, Y. Peng, and X. Peng, “Minimizing building electricity costs in a dynamic power market: Algorithms and impact on energy conservation,” in *2013 IEEE 34th Real-Time Systems Symposium*, Dec. 2013, pp. 107–117.

[35] L. Lan and Y. K. Tan, “Advanced building energy monitoring using wireless sensor integrated energyplus platform for personal climate control,” in *2015 IEEE 11th International Conference on Power Electronics and Drive Systems*, Jun. 2015, pp. 567–574.

[36] U. Manandhar, A. Ukil, and D. Wang, “Building hvac load profiling using energyplus,” in *2015 IEEE Innovative Smart Grid Technologies - Asia (ISGT ASIA)*, Nov. 2015, pp. 1–6.

[37] N. Kruis, “Reconciling differences between residential dx cooling models in doe-2 and energyplus,” *Proceedings of SimBuild*, vol. 4, no. 1, pp. 134–141, 2010.

[38] R. Fourer, D. M. Gay, and B. W. Kernighan, *AMPL: A modeling language for mathematical programming*, 2nd ed. Pacific Grove, CA: Brooks/Cole-Thomson Learning, 2003.

[39] *CPLEX Optimization subroutine library guide and reference*, CPLEX division ed., ILOG Inc., Incline Village, NV, 2008.

[40] U.S. Department of Energy. (2017, Oct.) Weather data by location. [Online]. Available: https://energyplus.net/weather-location/south_america_wmo_region_3/BRA//BRA_SP_Sao.Paulo.837810_INMET

[41] ANSI/ASHRAE, *Standards 55-1992, Thermal Environmental Conditions for Human Occupancy*, Std., 1992.

[42] J. C. S. Goncalves, N. S. Vianna, and N. C. da Silva Moura, *Iluminação natural e artificial*, PROCEL EDIFICA, Rio de Janeiro, Aug. 2011.

[43] Agência Nacional de Energia Elétrica – ANEEL, “Procedimentos de distribuição de energia elétrica no sistema elétrico nacional – prodist módulo 8 – qualidade da energia elétrica,” Brasílisa, 2015. [Online]. Available: http://www.aneel.gov.br/documents/656827/14866914/M%C3%B3dulo8_Revisao_8/9c78cfab-a7d7-4066-b6ba-cfbda3058d19

[44] A. Wachter and L. T. Biegler, “On the implementation of an interior-point filter line-search algorithm for large-scale nonlinear programming,” *Math. Prog.*, vol. 106, no. 1, pp. 25–57, 2006.

[45] F. Oldewurtel, A. Parisio, C. N. Jones, D. Gyalistras, M. Gwerder, V. Stauch, B. Lehmann, and M. Morari, “Use of model predictive control and weather forecasts for energy efficient building climate control,” *Energy and Buildings*, vol. 45, pp. 15 – 27, Feb. 2012.

[46] S. Hanif, H. B. Gooi, T. Massier, T. Hamacher, and T. Reindl, “Distributed congestion management of distribution grids under robust flexible buildings operations,” *IEEE Trans. Power Syst.*, vol. 32, no. 6, pp. 4600–4613, Nov. 2017.

[47] H. Wang, K. Meng, Z. Y. Dong, Z. Xu, F. Luo, and K. P. Wong, “Efficient real-time residential energy management through milp based rolling horizon optimization,” in *2015 IEEE Power Energy Society General Meeting*, Jul. 2015, pp. 1–6.

[48] R. Palma-Behnke, C. Benavides, F. Lanas, B. Severino, L. Reyes, J. Llanos, and D. Sáez, "A microgrid energy management system based on the rolling horizon strategy," *IEEE Transactions on Smart Grid*, vol. 4, no. 2, pp. 996–1006, Jun. 2013.

[49] J. Silvente, G. M. Kopanos, E. N. Pistikopoulos, and A. Espuña, "A rolling horizon optimization framework for the simultaneous energy supply and demand planning in microgrids," *Applied Energy*, vol. 155, no. 1, pp. 485 – 501, Oct. 2015.

Appendix

APPENDIX A – Buildings and Microgrid Features.

A.1 Buildings Features

Specific information of the zones of the buildings is presented in Tables 9–11. The three buildings studied correspond to toy models that were develop based on the default information used by EnergyPlus. The HVAC capacity of each zone was estimated using the sizing tool of EnergyPlus, while LP_z was calculated according to the type of each zone.

Table 9 – Characteristics of the zones of Building 1

z	Tag	Area [m^2]	Electric devices	Persons	HVAC capacity [BTU]	LP_z [W/Lx]
1	Office 202	50	9	10	24 000	1.5
2	Classroom 201	50	6	30	2*24 000	2.0
3	Classroom 203	43	5	26	18 000/24 000	1.7
4	Classroom 103	43	5	26	36000	1.7
5	Computing room 204	63	17	16	2*24 000	1.9
6	Computing room 104	63	17	16	36 000	1.9
7	Classroom 102	35	4	21	24 000	1.4
8	Classroom 205	35	4	21	30 000	1.4
9	Meetingroom	35	6	7	24 000	1.1
10	Office 101	35	6	7	18 000	1.1

Table 10 – Characteristics of the zones of Building 2

z	Tag	Area [m^2]	Electric devices	Persons	HVAC capacity [BTU]	LP_z [W/Lx]
10	Computing room 107	111	14	22	3*18 000	3.3
9	Computing room 106	67	8	13	24 000	2.0
8	Conference room	57	7	11	36 000	1.7
7	Office 109	41	5	8	18 000	1.2
6	Office 108	41	5	8	18 000	1.2
5	Computing room 105	84	10	17	36 000	2.5
4	Computing room 104	72	9	14	30 000	2.2
3	Computing room 103	65	8	13	30 000	2.0
2	Computing room 102	72	9	14	30 000	2.2
1	Computing room 101	84	10	17	18 000/24 000	2.5

Table 11 – Characteristics of the zones of Building 3

z	Tag	Area [m^2]	Electric devices	Persons	HVAC capacity [BTU]	LP_z [W/Lx]
10	Office 106	68	9	17	36 000	2.1
9	Office 105	84	11	8	30 000	2.5
8	Office 104	67	8	7	24 000	2.0
7	Office 103	56	7	6	18 000	1.7
6	Classroom 110	60	8	15	30 000	1.8
5	Classroom 109	76	10	19	36 000	2.3
4	Classroom 108	63	8	14	24 000	1.7
3	Classroom 107	60	8	15	30 000	1.8
2	Office 102	30	4	3	12 000	0.9
1	Office 101	34	4	3	12 000	1.0

Fig. 31 shows the occupancy profile of the zones of the buildings. Different occupancy patterns were assigned to the zones regarding their final use.

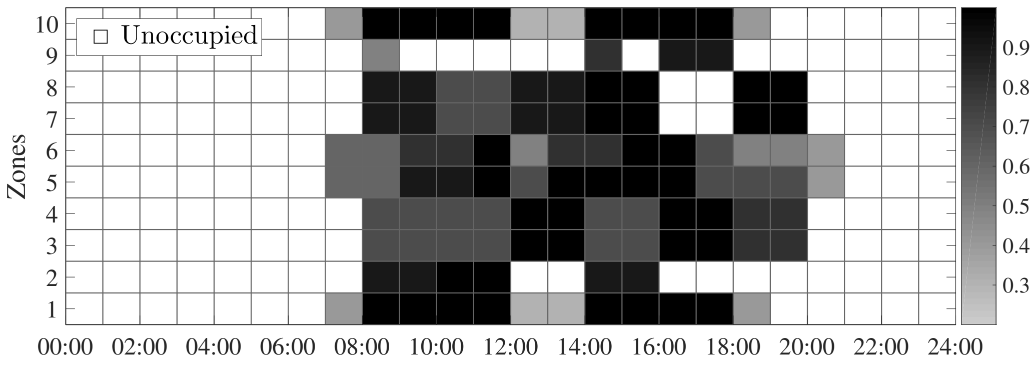

(a) Building 1.

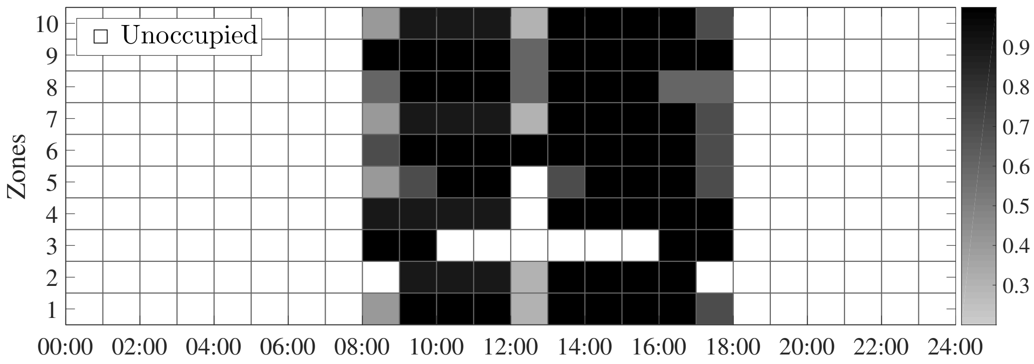

(b) Building B2.

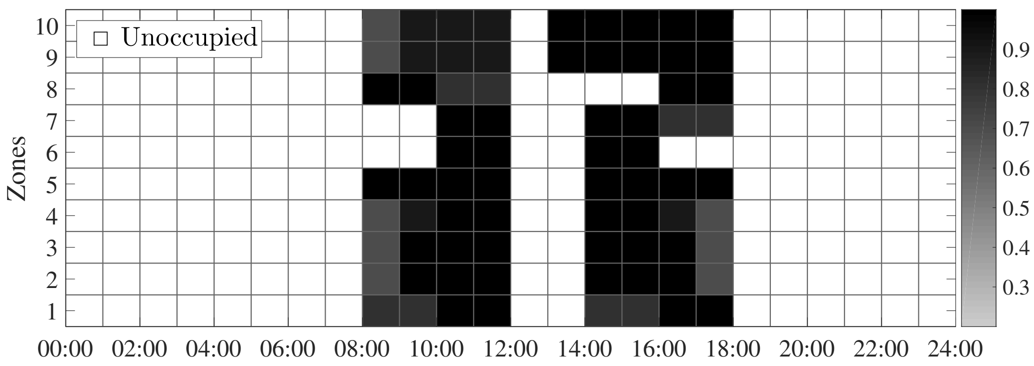

(c) Building B3.

Figure 31 – Occupancy profile of the buildings analyzed.

Fig. 32 shows the electrical devices usage profile of the zones of the buildings. These profiles are linked to the occupancy patterns already presented and were assigned to the zones regarding their final use.

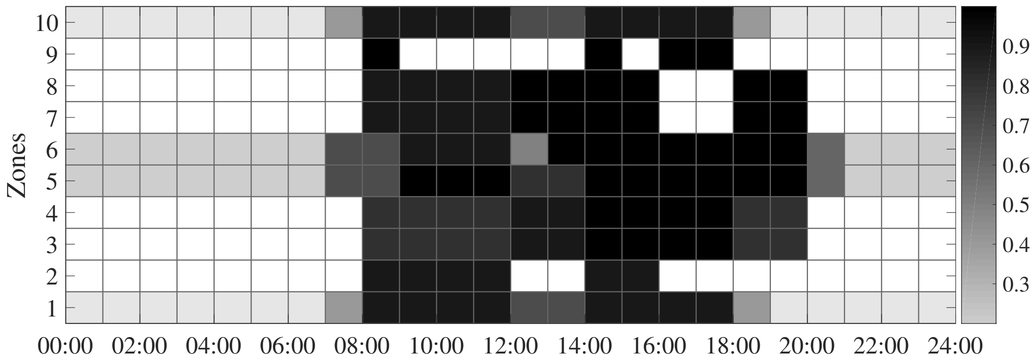

(a) Building 1.

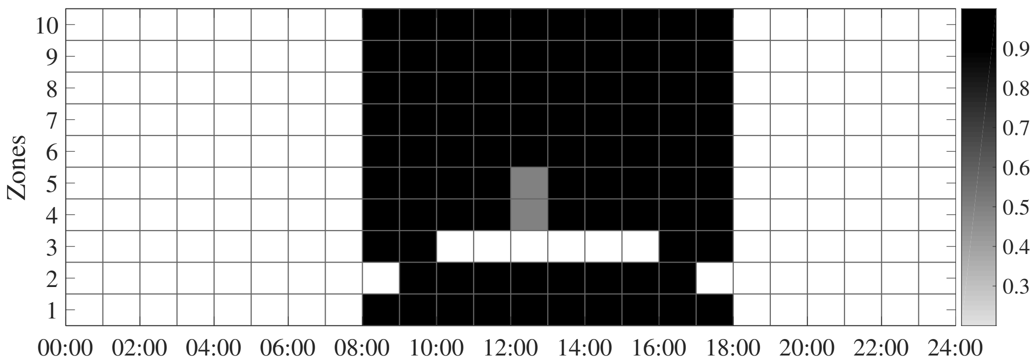

(b) Building B2.

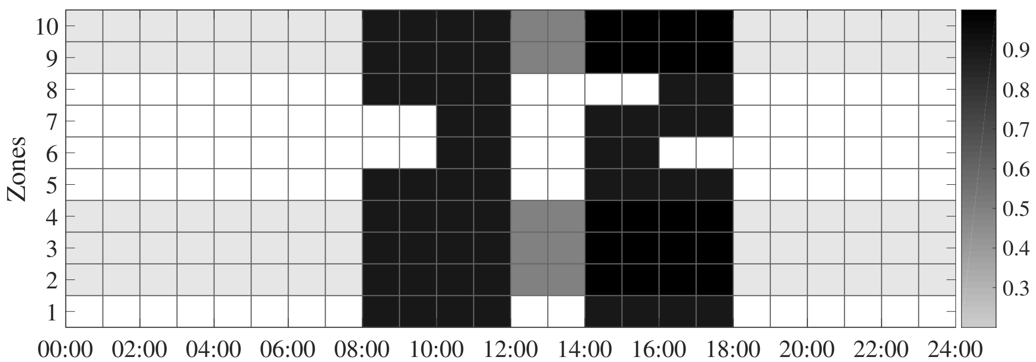

(c) Building B3.

Figure 32 – Electrical devices usage profile of the buildings analyzed.

A.2 Microgrid Features

The microgrid test case is based on the topology of the IEEE 13 node test feeder. The nominal voltage of the microgrid is 4.16 [kV], table 12 presents the impedance and current capacity of each branch of the grid. Table 13 contains the information related to the buses.

Table 12 – Impedance and current capacity of branches

From i	To j	$R_{i,j}$ [Ω]	$X_{i,j}$ [Ω]	$\overline{I}^{sqr}_{i,j}$ [A]
1	2	0.6114	0.9597	250
2	3	0.1528	0.2399	100
2	5	0.1528	0.2399	100
2	7	0.6114	0.9597	100
3	4	0.0918	0.1440	50
5	6	0.2446	0.3842	20
7	8	0.0918	0.1440	80
7	11	0.3057	0.4798	20
7	12	0.0918	0.1440	25
8	9	0.0918	0.1440	80
8	10	0.2446	0.3842	15
12	13	0.1528	0.2399	15

Table 13 – Buses types (1=Substation, 2=Building, 0=Load)

Bus	Type	Description
1	1	Substation
2	0	—
3	0	Load 3
4	0	Load 4
5	0	Load 5
6	2	Building 6
7	0	—
8	2	Building 8
9	0	Load 9
10	2	Building 10
11	2	Building 11
12	2	Building 12
13	2	Building 13